Title
Giant Outer Transiting Exoplanet Mass (GOT 'EM) Survey. II. Discovery of a Failed Hot Jupiter on a 2.7 Yr, Highly Eccentric Orbit* * Some of the data presented herein were obtained at the W. M. Keck Observatory, which is operated as a scientific part...

Journal
The Astronomical Journal, 162(4)

ISSN
0004-6256

Authors
Dalba, Paul A
Kane, Stephen R
Li, Zhexing
et al.

Publication Date
2021-10-01

DOI
10.3847/1538-3881/ac134b

Peer reviewed

DRAFT VERSION MARCH 8, 2021
Typeset using LATEX **twocolumn** style in AASTeX63

Giant Outer Transiting Exoplanet Mass (GOT 'EM) Survey. II. Discovery of a Failed Hot Jupiter on a 2.7 Year, Highly Eccentric Orbit*

PAUL A. DALBA,[1,†] STEPHEN R. KANE,[1] ZHEXING LI,[1] MASON G. MACDOUGALL,[2] LEE J. ROSENTHAL,[3] COLLIN CHERUBIM,[3] HOWARD ISAACSON,[4,5] DANIEL P. THORNGREN,[6] BENJAMIN FULTON,[7] ANDREW W. HOWARD,[3] ERIK A. PETIGURA,[2] EDWARD W. SCHWIETERMAN,[1,8] DAN O. PELUSO,[5,9] THOMAS M. ESPOSITO,[9,10] FRANCK MARCHIS,[9,11] AND MATTHEW J. PAYNE[12]

[1]*Department of Earth and Planetary Sciences, University of California Riverside, 900 University Ave, Riverside, CA 92521, USA*
[2]*Department of Physics & Astronomy, University of California Los Angeles, Los Angeles, CA 90095, USA*
[3]*Department of Astronomy, California Institute of Technology, Pasadena, CA 91125, USA*
[4]*Department of Astronomy, University of California Berkeley, Berkeley CA 94720, USA*
[5]*Centre for Astrophysics, University of Southern Queensland, Toowoomba, QLD, Australia*
[6]*Institute for Research on Exoplanets (iREx), Université de Montréal, Canada*
[7]*NASA Exoplanet Science Institute/Caltech-IPAC, MC 314-6, 1200 E. California Blvd., Pasadena, CA 91125, USA*
[8]*Blue Marble Space Institute of Science, Seattle, WA, 98115*
[9]*SETI Institute, Carl Sagan Center, 189 Bernardo Avenue, Mountain View, CA, USA*
[10]*Astronomy Department, University of California, Berkeley, CA 94720, USA*
[11]*Unistellar, 198 Alabama Street, San Francisco CA 94110 USA*
[12]*Harvard-Smithsonian Center for Astrophysics, 60 Garden St., MS 51, Cambridge, MA 02138, USA*

Submitted to ApJ

ABSTRACT

Radial velocity (RV) surveys have discovered giant exoplanets on au-scale orbits with a broad distribution of eccentricities. Those with the most eccentric orbits are valuable laboratories for testing theories of high eccentricity migration. However, few such exoplanets transit their host stars thus removing the ability to apply constraints on formation from their bulk internal compositions. We report the discovery of KOI-375.01, a transiting 4 M_J giant planet on a 988.88 day orbit with the extreme eccentricity of $0.921^{+0.010}_{-0.015}$. Our decade-long RV baseline from the Keck I telescope allows us to measure the orbit and bulk heavy element composition of KOI-375.01 and place limits on the existence of undiscovered companions. KOI-375.01 is a failed hot Jupiter that was excited to high eccentricity by multiple scattering events that likely began during its gas accretion phase. Its final periastron distance is too large to allow for tidal circularization, so now it orbits it host from distances spanning 0.16–3.9 au. The swing in planetary equilibrium temperature resulting from this extreme orbit is over 700 K. A simulation of the thermal phase curve of KOI-375.01 during periastron passage demonstrates that it is a remarkable target for atmospheric characterization from the James Webb Space Telescope, which could potentially also measure the planet's rotational period as the hot spot from periastron rotates in and out of view. Continued characterization of the KOI-375 system stands to refine theories explaining the formation of hot Jupiters and cool giant planets like those in the solar system.

1. INTRODUCTION

Giant planet migration is typically invoked to explain the present day architecture of exoplanetary systems. Theories of planetary migration abound but can broadly be categorized as disk-driven migration, caused by torques from the protoplanetary disk (e.g., Goldreich & Tremaine 1980; Lin & Papaloizou 1986; Ward 1997; Baruteau et al. 2014), or high-eccentricity migration (HEM), whereby a giant planet exchanges orbital energy and angular momentum with one or more other objects in its system and subsequently experiences tidal circularization during close periastron passages

Corresponding author: Paul A. Dalba
pdalba@ucr.edu

* Some of the data presented herein were obtained at the W. M. Keck Observatory, which is operated as a scientific partnership among the California Institute of Technology, the University of California and the National Aeronautics and Space Administration. The Observatory was made possible by the generous financial support of the W. M. Keck Foundation.

† NSF Astronomy and Astrophysics Postdoctoral Fellow

(e.g., Rasio & Ford 1996; Wu & Murray 2003; Nagasawa et al. 2008; Wu & Lithwick 2011). The characterization of giant planets and their orbits offers a window into which mechanisms might have been at play.

The subject of HEM can itself be divided into multiple pathways including Kozai-Lidov oscillations (Kozai 1962; Lidov 1962) induced by a stellar companion (e.g., Wu & Murray 2003; Fabrycky & Tremaine 2007; Naoz et al. 2012) or planetary companion (e.g., Naoz et al. 2011; Lithwick & Naoz 2011), planet-planet scattering (e.g., Rasio & Ford 1996; Ford & Rasio 2006; Chatterjee et al. 2008; Jurić & Tremaine 2008; Raymond et al. 2010; Nagasawa & Ida 2011), and secular chaos (e.g., Wu & Lithwick 2011; Hamers et al. 2017). Each mechanism can excite the eccentricity of a giant planet and, in doing so, imprints identifying (although not necessarily unique) clues in the present-day system. Disentangling all the possible migration pathways for a single system or even determining the fraction of systems that migrated through various channels is challenging, though (e.g., Fabrycky & Winn 2009; Socrates et al. 2012; Dawson et al. 2015; Dawson & Murray-Clay 2013).

HEM theories are readily tested in systems containing hot Jupiters, giant planets on orbits shorter that $\sim$10 days that are thought to have formed at greater distances from their host stars (see Dawson & Johnson 2018, for a recent review). In addressing the mysteries of giant planet HEM, it is beneficial not only to investigate these hot giant planets themselves but also *proto-* and *failed* hot Jupiters, objects in the process of becoming hot Jupiters and those that followed a similar evolutionary pathway but will not become hot Jupiters, respectively. HD 80606 b (e.g., Naef et al. 2001; Moutou et al. 2009; Winn et al. 2009) is possibly a proto-hot Jupiter caught in the act of tidal circularization (e.g., Wu & Murray 2003; Fabrycky & Tremaine 2007; Socrates et al. 2012). Motivated by this planet, Socrates et al. (2012) theorized that if HEM is the preferred pathway of hot Jupiter migration, then the *Kepler* mission (Borucki et al. 2010) should detect a population of highly eccentric ($e > 0.9$) giant planets, and their current orbital periods (P) should distinguish which are likely to be proto-hot Jupiters ($P \lesssim 2$ years) or failed hot Jupiters ($P \gtrsim 2$ years). This theory was supported by the detection of highly eccentric eclipsing binaries by *Kepler* (Dong et al. 2013). However, similar support was not offered by the *Kepler*'s planet discoveries. Based on analysis of the photo-eccentric effect (Dawson & Johnson 2012), Dawson et al. (2015) reported a paucity of proto-hot Jupiters on highly eccentric orbits in the *Kepler* sample even after considering the limited sensitivity of transit surveys to planets with orbital distances of a few au. This work instead suggested that disk migration was the dominant pathway of hot Jupiter formation. Only one proto-hot Jupiter candidate was identified (Kepler-419 b; Dawson et al. 2012), which was later refined with radial velocity (RV) observations to be a failed hot Jupiter (Dawson et al. 2014).

Although RV surveys have detected a handful of failed hot Jupiter exoplanets, Kepler-419 b stands alone owing to its transiting geometry. By definition, a failed hot Jupiter must have a sufficiently wide orbit such that its periastron distance (despite its high eccentricity) is too large for tidal forces to efficiently circularize its orbit. By the observational biases of the transit method (e.g., Beatty & Gaudi 2008), such long-period planets are unlikely to be observed in transit (e.g., Dalba et al. 2019), although eccentricity can increase this probability (e.g., Kane 2007). According to the NASA Exoplanet Archive[1], of the 16 non-controversial exoplanets with measured eccentricity above 0.8, only Kepler419 b, HD 80606 b, and Kepler-1656 b (Brady et al. 2018) have measured radii. Increasing this threshold to $e > 0.9$ leaves only HD 80606 b.

Those rare few eccentric, long-period giant exoplanets that do transit their hosts are exceptionally valuable because their radii and bulk compositions provide new windows into their formation and migration. Metal-rich stars preferentially host eccentric hot Jupiters (Dawson & Murray-Clay 2013; Buchhave et al. 2018), lending credence theories of planet-planet scattering since host star metallicity is known to correlate with giant planet occurrence (e.g., Gonzalez 1997; Santos et al. 2004; Fischer & Valenti 2005). Furthermore, empirical trends in giant planet metal enrichment (relative to stellar) with planet mass hint at a fundamental and expected connection between the metal content of stars and their planets (Miller & Fortney 2011; Thorngren et al. 2016; Teske et al. 2019). With this in mind, giant planet bulk metallicity is likely a key piece on information when piecing together migration history (e.g., Alibert et al. 2005; Ginzburg & Chiang 2020; Shibata et al. 2020).

As the second discovery of the Giant Outer Transiting Exoplanet Mass (GOT 'EM) survey (Dalba et al. 2021), we present a new failed hot Jupiter from the *Kepler* sample: KOI-375.01 (hereafter KOI-375.01 as we will confirm its planetary nature[2]). In Section 2, we show the observations of this system including photometry from the *Kepler* spacecraft that detected two transits spaced by 989 days, follow-up adaptive optics (AO) imaging, and a follow-up Doppler spectroscopy campaign spanning a decade. In Section 3, we combine these data sets through a comprehensive modeling of system parameters using EXOFASTv2 (Eastman et al. 2013, 2019). In Section 4, we conduct a thorough analysis to rule out the presence of planetary or stellar companions across a wide swath of parameter space, which has important impli-

[1] Accessed 2021 February 2 (https://exoplanetarchive.ipac.caltech.edu/).

[2] We will revise this to the Kepler name at a later date when a number is assigned

cations for the migration history of KOI-375.01. We also retrieve this planet's bulk metallicity and simulate its reflected light phase curve, the detection of which would be an unprecedented discovery that is within the anticipated capability of the *James Webb Space Telescope* (*JWST*). In Section 5, we offer our interpretation of all of the analyses of the KOI-375 system in regards to the formation history of KOI-375.01 and motivate a campaign to measure the stellar obliquity during a future transit. Finally, in Section 6, we summarize our findings.

2. OBSERVATIONS

We employ photometric, spectroscopic, and imaging observations in this analysis of the KOI-375 system. In the following sections, we describe how each of these data sets was collected and processed.

2.1. *Photometric Data from Kepler*

The *Kepler* spacecraft observed KOI-375 at 30-minute cadence in all 18 quarters of its primary mission. We accessed the Pre-search Data Conditioning Simple Aperture Photometry (PDCSAP; Jenkins et al. 2010; Smith et al. 2012; Stumpe et al. 2012) through the Mikulski Archive for Space Telescopes (MAST), stitching together the light curves from individual quarters into one time series with a common baseline flux using lightkurve (Lightkurve Collaboration et al. 2018). We further cleaned the photometry by removing all data points flagged for "bad quality" and dividing out the median background flux to produce a normalized light curve. We then measured a preliminary time of conjunction, duration, and period for the transiting planet using a box least squares transit search (BLS; Kovács et al. 2002), identifying only two transit events in Quarters 2 and 13. The time separating these two transits was 989 days, the suspected orbital period of KOI-375.01. However, the data gap between Quarters 7 and 8 occurred precisely in between these transits, introducing a ~494-day orbital period alias.

We used the BLS results to mask out both transits and detrend any variability in the light curve without risk of obscuring the signal. Interpolating over the masked transit events, we fit a smoothed curve to systematics in the photometry using a Savitzky-Golay filter (Virtanen et al. 2020) and then subtracted out this additional structure to produce our final data product. Before unmasking the transit events, we clipped any remaining individual outliers with residuals to the smoothed fit that were greater than 3-σ discrepant.

We present the binned, detrended *Kepler* transits of KOI-375.01 in Figure 1. Under the assumption of a circular edge-on orbit, the mean transit duration of KOI-375.01 and stellar properties reported by the NASA Exoplanet Archive suggest an orbital period of approximately 11 days. This scenario is thoroughly ruled out by the extensive *Kepler* data set. Instead, we explored the possibility that orbital eccentricity affected the duration of the transit.

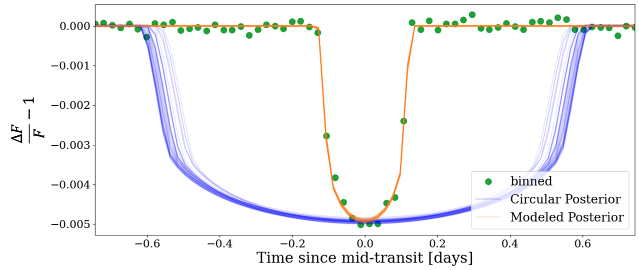

Figure 1. Phase-folded, binned *Kepler* data for KOI-375.01 (green dots). The transit duration is substantially shorter than expected for a circular orbit (blue models) and is better reproduced by models with high eccentricity (orange lines).

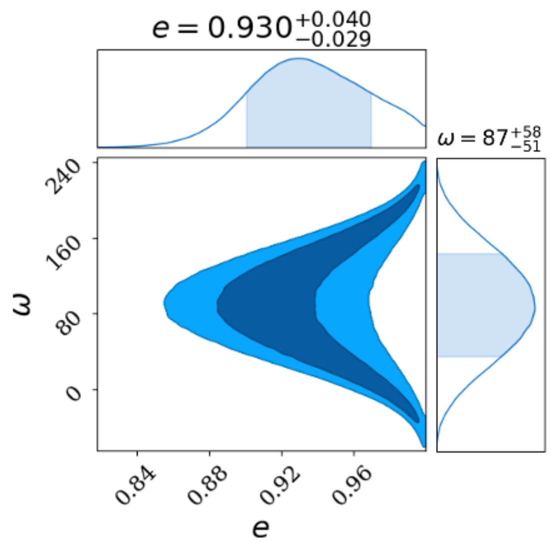

Figure 2. Posterior probabilities distributions for orbital eccentricity (e) and argument of periastron (ω, in degrees) from the photoeccentric modeling. Values reported are the median and 68% credible intervals.

2.1.1. *Photoeccentric Transit Modeling*

The observed transits of KOI-375.01 have a duration of ~6 hours, which is nearly 5 times shorter than would be expected for a Jovian-size planet at such a large separation (assuming a period of ~989 days). The two plausible sources of this discrepancy are high impact parameter (b) or high eccentricity (e), but a preliminary transit fit reveals that high b alone cannot account for the anomalously short transit duration. We instead developed a model to account for both of these properties through a photometric transit fit that takes into consideration the photo-eccentric framework of Dawson & Johnson (2012), as shown in Figure 1.

We modeled the standard transit parameters, including orbital period (P), time of conjunction (T_C), planet-star radius ratio ($R_p/R_\star$), and b, along with the expected stellar density assuming a circular orbit, $\rho_{\star,\rm circ}$, to obtain a model that encodes information about the true orbital eccentricity of the planet according to Kipping et al. (2012b). We derived this dynamical information from our results by comparing our modeled $\rho_{\star,\rm circ}$ to the true stellar density, $\rho_\star$, represented by the median of our EXOFASTv2 $\rho_\star$ posterior (Section 3). A value of $\rho_{\star,\rm circ}$ greater than $\rho_\star$ would imply that the planet transited faster than expected and vice versa, given an initial assumption of $e = 0$. Breaking from this assumption, however, we calculated which values of e and the argument of periastron (ω) were necessary to account for the unusually fast transit, subsequently bringing $\rho_{\star,\rm circ}$ into closer agreement with $\rho_\star$. For both parameters, we calculated posterior probability distributions using the log-likelihood function (Dawson & Johnson 2012)

$$\log P(e,\omega|\rho_\star,\rho_{\star,\rm circ}) \propto -\frac{1}{2}[g(e,\omega)^3\rho_\star - \rho_{\star,\rm circ}]^2 \quad (1)$$

where

$$g(e,\omega) = \frac{1+e\sin\omega}{\sqrt{1-e^2}}\ , \quad (2)$$

following the notation of Kipping (2010) and Kipping et al. (2012b).

Constraints on ω using this method tend to be broad, but they are sufficient to determine if a transit occurs closer to periastron (as is the case for KOI-375.01) or apastron. On the other hand, we were able to constrain the eccentricity of KOI-375.01 here with high certainty. We found that the 68% credible interval for eccentricity is 0.901–0.970 (Figure 2).

In a previous analysis of the photoeccentric effect in *Kepler* transit data, Dawson et al. (2015) found 0^{+1}_{-0} giant planets on highly eccentric orbits that are likely undergoing tidal circularization. This non-detection refuted the hypothesis of Socrates et al. (2012) that approximately four such planets should be detected assuming that HEM is the dominant hot Jupiter migration scenario. In the case of KOI-375.01, our photoeccentric modeling represents an update to their analysis using more recent stellar information.

Assuming tidal decay at constant angular momentum, the highest allowed values of eccentricity from our photoeccentric modeling would produce a final orbital period below 10 days, the canonical threshold for hot Jupiters. Therefore, based on just this photoeccentric effect analysis, KOI-375.01 is a candidate proto-hot Jupiter. However, additional orbital characterization via RV monitoring of the host is needed to refine the eccentricity and the nature of KOI-375.01.

2.2. *Spectroscopic Data from HIRES*

We acquired 15 high resolution spectra of KOI-375 with HIRES (Vogt et al. 1994) on the Keck I telescope in support of our Doppler monitoring of the KOI-375 system. The baseline of these observations spans nearly a decade. For each observation, the starlight passed through a heated iodine cell before reaching the slit to enable the precise wavelength calibration of each RV measurement.

We did not acquire a high signal-to-noise (S/N) "template" spectrum as is typical for HIRES RV observations (e.g., Howard et al. 2010). Instead, we identified a pre-existing, best match template spectrum in the HIRES spectral library following Dalba et al. (2020a). The best match star was HD 203473, a brighter G6V star with similar spectroscopic properties to KOI-375 according to a SpecMatch–Emp[3] analysis (Yee et al. 2017). The use of a best match template incurs extra uncertainty in addition to internal RV errors. Following conservative estimations by Dalba et al. (2020a, see their Table 2), we added 6.2 m s^{-1} to our internal RV errors in quadrature to account for this method. After swapping in the template of HD 203473, the RV extraction proceeded following the standard forwarding techniques employed the by California Planet Search (e.g., Howard et al. 2010; Howard & Fulton 2016).

We list the full RV data set for KOI-375 in Table 1. The uncertainties listed include the additional uncertainty incurred by the matched-template method of RV extraction (Dalba et al. 2020a). We also include corresponding $S_{\rm HK}$ activity indicators derived from the Ca II H and K spectral lines (Wright et al. 2004; Isaacson & Fischer 2010).

We note that the first RV measurement (from BJD=2455669) is the least precise observation in the series. Its uncertainty is three standard deviations above the mean. This larger error is not surprising as the exposure time for the spectrum used to measure that RV was substantially shorter than the others. The resulting best fit velocity in each two-angstrom chunk of spectrum, which typically only contain one stellar and one iodine line, was less precise, leading to the larger error on RV. When folded on the ephemeris of KOI-375.01, this data point occupies a non-critical phase in the orbit. However, this data point extends the baseline of RVs observations by 826 days and is critical to our consideration of acceleration in the KOI-375 system (Section 4.2). Although there is no obvious reason to exclude this data point from our analysis besides its larger uncertainty, we will treat this data point with skepticism moving forward.

In Section 3, we model the RVs and transits simultaneously, confirming that the orbital period of KOI-375.01 is accurately represented by the time elapsed between the two *Kepler* transits (988.88 days) and not half of that value. Visual inspection of the RV data listed in Table 1 folded on an orbital period of 494.44 days suggests no Keplerian signal

[3] https://github.com/samuelyeewl/specmatch-emp

Table 1. RV Measurements of KOI-375

BJD_{TDB}	RV (m s^{-1})	S_{HK}
2455669.111196	25.3±8.5	0.0966±0.0010
2456495.013178	28.9±6.8	0.1220±0.0010
2456532.811313	31.3±6.8	0.1330±0.0010
2458383.894210	16.2±7.5	0.1609±0.0010
2458593.029972	38.6±6.8	0.1172±0.0010
2458679.811045	63.2±6.8	0.1260±0.0010
2458765.877254	68.1±6.8	0.1311±0.0010
2458815.758493	90.0±7.2	0.1267±0.0010
2459006.997818	195.5±6.8	0.1222±0.0010
2459038.992753	−118.9±6.9	0.1222±0.0010
2459041.035816	−119.9±7.1	0.1205±0.0010
2459051.874260	−93.1±6.7	0.1265±0.0010
2459070.992339	−72.1±7.2	0.0964±0.0010
2459189.758826	−31.5±7.6	0.1183±0.0010

at this periodicity. Therefore, we hereafter do not consider the possibility that another transit occurred during the gap in observations between *Kepler* quarters 7 and 8.

2.3. *Archival AO Imaging*

The KOI-375 system has been observed in several imaging campaigns previously (see Furlan et al. 2017, for a summary). To explore the existence of bound or background stellar neighbors, we present three data sets acquired from the Exoplanet Follow-up Observing Program[4].

The first imaging data set comprises AO images from the PHARO instrument (Hayward et al. 2001) at the 200 inch telescope at Palomar Observatory as published by Wang et al. (2015a). This work used a 3-point dither pattern to obtain a set of images in the K_s band that were then combined and searched for stellar companions (Figure 3, left panel). Based on these observations, Wang et al. (2015a) claimed two detections: one source with $\Delta K_s = 3.3$ with a separation and position angle (PA) of $5''.47$ and 157.0°, respectively; and another source with $\Delta K_s = 4.6$ with a separation and PA of $3''.19$ and 305.5°, respectively. Both detections are visible in the left panel of Figure 3. The source with PA=157.0° (indicated by a green, vertical arrow) is resolved by Gaia (Gaia Collaboration et al. 2016, 2020) and has the EDR3 source ID of 2136191732305041920 (hereafter *Gaia-213* for simplicity). The parallax and proper motion of KOI-375 and *Gaia-213* as measured by Gaia definitively show that these two stars are not gravitationally associated. The other source claimed by Wang et al. (2015a) as well as a brighter source near the upper edge of the image that was not claimed by Wang et al. (2015a) (indicated by yellow, horizontal arrows) are not present in the Gaia EDR3 catalog.

The second imaging data set also comprises AO images from the PHARO instrument but in the Br-γ filter and published by Furlan et al. (2017). Surprisingly, only KOI-375 and *Gaia-213* (at PA=157.0°) are visible despite deeper magnitude limits near $3''.19$: $\Delta K_s = 4.9$ versus ΔBr-$\gamma = 7.0$ (Wang et al. 2015a; Furlan et al. 2017). The time elapsed between the epochs of imaging, roughly one month, is also too short to explain the discrepancy.

The solution to this conundrum lies in the relative positioning of the two sources in question relative to the positioning of KOI-375 and *Gaia-213*. The separation and PA between the two pairs are identical. Visual inspection also suggests that the contrast between the stars in each pair is also similar. Thus, our conclusion is that the two sources identified by yellow, horizontal arrows in Figure 3 are spurious duplications of KOI-375 and *Gaia-213* caused by an accidental image alignment error.

The third imaging data set comprises AO images from the NIRC2 instrument (Wizinowich et al. 2000) at the Keck II telescope at W. M. Keck Observatory as published by Furlan et al. (2017). Observations were taken in the Br-γ filter and the field of view was too small to include any of the other sources (astrophysical or spurious) mentioned previously (Figure 4). The NIRC2 data yield a non-detection of a stellar neighbor within $2''$ with delta-magnitude limits of 8.4 and 8.7 at separations of $0''.5$ and $1''.0$, respectively (Furlan et al. 2017). Since the NIRC2 observations of KOI-375 provide the strongest constraints on neighboring stars, we continue our analysis using only these data.

We used the NIRC2 contrast curve (i.e., 5σ limiting delta-magnitude as a function of separation) to derive the corresponding limiting mass for a bound companion. First, we downloaded a MESA Isochrones and Stellar Tracks (MIST) isochrone (Paxton et al. 2011, 2013, 2015; Dotter 2016; Choi et al. 2016) from the MIST web interpolator[5]. We provided values of initial stellar metallicity, extinction, and age based on the system modeling described in Section 3. This isochrone provide a numerical relationship between stellar mass and absolute K_s magnitude, which we treated interchangeably with Br-γ. After converting absolute magnitude to apparent magnitude (using the distance from Section 3), we interpolated the ΔK_s values with those measured by NIRC2 to calculate an upper limit of companion mass as a function of projected separation (Figure 4). At wider separations, the delta-magnitude values exceeded those in the MIST isochrone. For those separations we instead interpolated a

[4] ExoFOP, accessed 2021 February 5 (https://exofop.ipac.caltech.edu/).

[5] Accessed 2020 December 17 (http://waps.cfa.harvard.edu/MIST/).

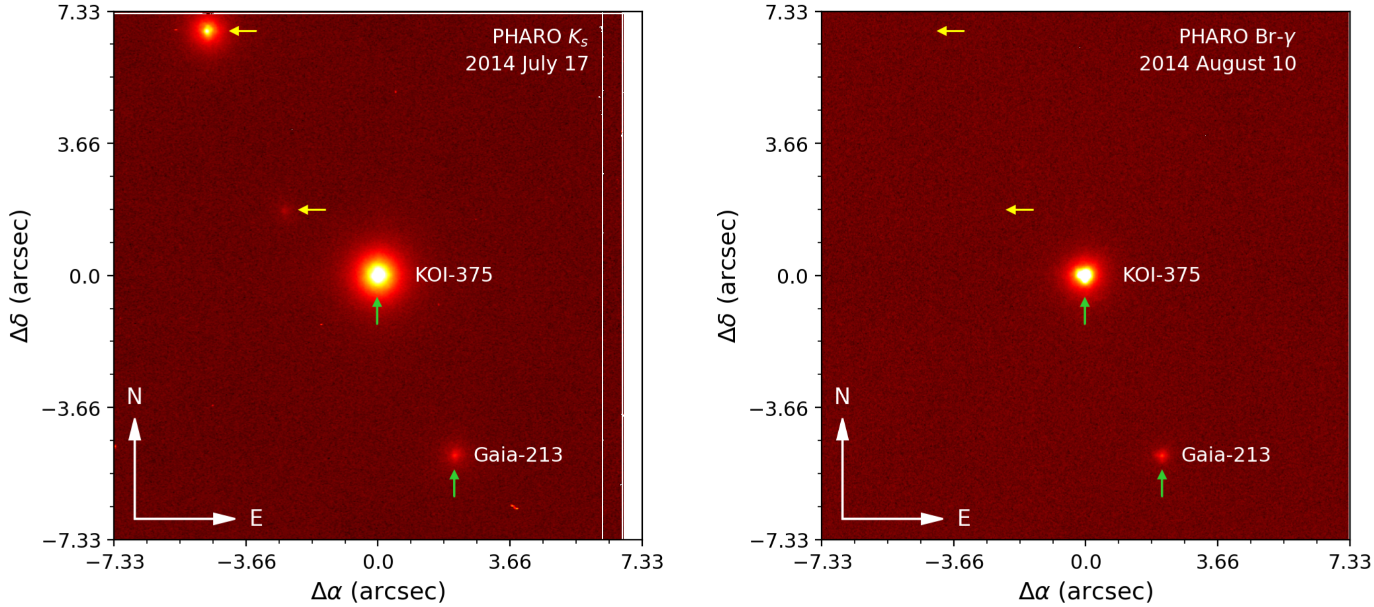

Figure 3. AO images of KOI-375 taken with the PHARO instrument on the 200 inch telescope at Palomar Observatory and acquired from ExoFOP. *Left:* Observation from Wang et al. (2015a) showing KOI-375 and three other sources. Green, vertical arrows identify KOI-375 (at center) and *Gaia-213* (see text), as resolved by Gaia. Yellow, horizontal arrows identify two additional source (not resolved by Gaia), the fainter of which was claimed as a detection by Wang et al. (2015a). The white stripes on the eastern edge of the image are artifacts from the mosaicking. *Right:* Observation from Furlan et al. (2017) showing KOI-375 at center and *Gaia-213*. In both images, the scales and locations of the arrows are identical. The two sources present in the left panel that are absent in the right panel are an spurious duplication of KOI-375 and *Gaia-213* caused by an alignment error. According to Gaia astrometry, *Gaia-213* is not gravitationally bound to KOI-375.

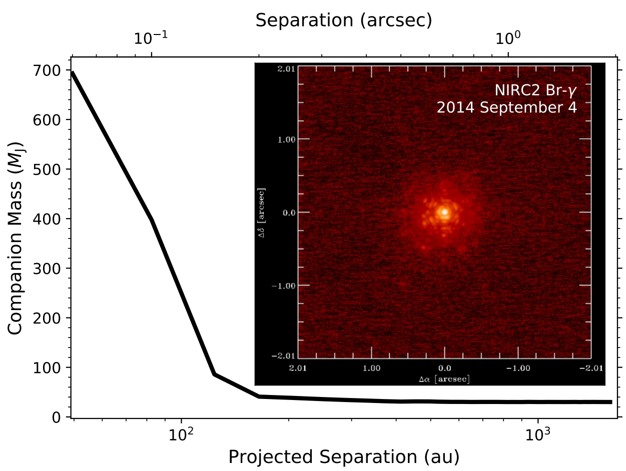

Figure 4. Upper limit on companion mass in the KOI-375 system based on the contrast curve measured from NIRC2 AO images. The masses were estimated by interpolating a MIST isochrone (in the stellar regime) and a brown dwarf isochrone (in the substellar regime). The inset is the NIRC2 image of KOI-375 published by Furlan et al. (2017).

5 Gyr brown dwarf isochrone from Baraffe et al. (2003). Beyond a projected separation of ∼200 au, we find that any companion in the KOI-375 system must have a mass below $\sim 32\ M_J$.

3. MODELING THE STELLAR AND PLANETARY PARAMETERS

We simultaneously fit models to the transit and RV data for KOI-375 while also modeling the stellar spectral energy distribution (SED) using archival broadband photometry using the EXOFASTv2 suite. The result was a set of precise, consistent stellar (Table 2) and planetary (Table 3) parameters.

We began by defining informative priors on several stellar parameters, which are listed at the top of Table 2. We constrained stellar effective temperature ($T_{\rm eff}$) and metallicity (as described by [Fe/H]) based on a SpecMatch[6] analysis (Petigura 2015; Petigura et al. 2017) of a moderate S/N (∼40) spectrum of KOI-375 acquired with Keck-HIRES without the iodine cell. This analysis produced an uncertainty on $T_{\rm eff}$ of 100 K, which we inflated to 115 K, in line with the systematic uncertainty floor reported by Tayar et al. (2020). The SpecMatch analysis also suggested that the stellar radius is $\sim 1.7\ R_\odot$, hinting that this G2 star has evolved off of the main sequence (see Section 3.1). In addition to $T_{\rm eff}$ and [Fe/H], we constrained the upper limit on V-band extinction using the galactic reddening maps of Schlafly & Finkbeiner (2011). Lastly, we constrained the parallax of KOI-375 as measured by Gaia in EDR3 (Gaia Collaboration et al. 2016,

[6] https://github.com/petigura/specmatch-syn

Table 2. Median values and 68% confidence intervals for the stellar parameters for KOI-375.

Parameter	Units	Values
Informative Priors:		
$T_{\rm eff}$	Effective Temperature (K)	$\mathcal{N}(5772, 115)$
[Fe/H]	Metallicity (dex)	$\mathcal{N}(0.2, 0.06)$
ϖ	Parallax (mas)	$\mathcal{N}(1.213, 0.016)$
A_V	V-band extinction (mag)	$\mathcal{U}(0, 0.2902)$
Stellar Parameters:		
M_*	Mass ($M_\odot$)	$1.131^{+0.040}_{-0.051}$
R_*	Radius ($R_\odot$)	$1.697^{+0.058}_{-0.059}$
L_*	Luminosity ($L_\odot$)	$2.83^{+0.17}_{-0.19}$
F_{Bol}	Bolometric Flux (cgs)	$1.333\times10^{-10}{}^{+7.3\times10^{-12}}_{-8.5\times10^{-12}}$
ρ_*	Density (g cm^{-3})	$0.325^{+0.036}_{-0.032}$
$\log g$	Surface gravity (cgs)	4.031 ± 0.032
$T_{\rm eff}$	Effective Temperature (K)	5745^{+88}_{-89}
[Fe/H]	Metallicity (dex)	0.196 ± 0.057
[Fe/H]$_0$	Initial Metallicity^a	$0.218^{+0.054}_{-0.055}$
Age	Age (Gyr)	$7.4^{+1.5}_{-1.0}$
EEP	Equal Evolutionary Phase^b	$453.0^{+4.5}_{-5.8}$
A_V	V-band extinction (mag)	$0.187^{+0.068}_{-0.091}$
σ_{SED}	SED photometry error scaling	$1.05^{+0.42}_{-0.26}$
ϖ	Parallax (mas)	1.213 ± 0.016
d	Distance (pc)	825 ± 11

See Table 3 in Eastman et al. (2019) for a detailed description of all parameters and all default (non-informative) priors beyond those specified here. $\mathcal{N}(a,b)$ denotes a normal distribution with mean a and variance b^2. $\mathcal{U}(a,b)$ denotes a uniform distribution over the interval [a,b].

[a] Initial metallicity is that of the star when it formed.

[b] Corresponds to static points in a star's evolutionary history. See Section 2 of Dotter (2016).

Table 3. Median values and 68% confidence interval of the planet parameters for KOI-375.01.

Parameter	Units	Values
P	Period (days)	$988.88113^{+0.00091}_{-0.00092}$
R_P	Radius (R_J)	$1.065^{+0.043}_{-0.041}$
M_P	Mass (M_J)	$3.96^{+0.20}_{-0.19}$
T_C	Time of conjunction (BJD$_{\rm TDB}$)	$2455071.68459^{+0.00062}_{-0.00064}$
a	Semi-major axis (au)	$2.026^{+0.024}_{-0.031}$
i	Inclination (degrees)	$89.01^{+0.59}_{-0.27}$
e	Eccentricity	$0.921^{+0.010}_{-0.015}$
ω_*	Argument of Periastron^a (degrees)	$83.0^{+4.5}_{-4.9}$
$T_{\rm eq}$	Equilibrium temperature^b (K)	$253.8^{+3.7}_{-4.1}$
$\tau_{\rm circ}$	Tidal circularization timescale (Gyr)	$80000^{+150000}_{-46000}$
K	RV semi-amplitude (m s^{-1})	190^{+17}_{-16}
$\dot{\gamma}$	RV slope^c (m s^{-1} day^{-1})	$0.0031^{+0.0029}_{-0.0027}$
R_P/R_*	Radius of planet in stellar radii	$0.0644^{+0.0016}_{-0.0011}$
a/R_*	Semi-major axis in stellar radii	$256.4^{+9.3}_{-8.6}$
τ	Ingress/egress transit duration (days)	$0.0172^{+0.0039}_{-0.0022}$
T_{14}	Total transit duration (days)	$0.2502^{+0.0034}_{-0.0026}$
$T_{\rm FWHM}$	FWHM transit duration (days)	0.2326 ± 0.0017
b	Transit Impact parameter	$0.36^{+0.16}_{-0.24}$
b_S	Eclipse impact parameter	$7.6^{+2.4}_{-4.8}$
ρ_P	Density (g cm^{-3})	$4.06^{+0.54}_{-0.48}$
$logg_P$	Surface gravity (cgs)	$3.937^{+0.039}_{-0.040}$
$\langle F \rangle$	Incident Flux (10^9 erg s^{-1} cm^{-2})	$0.000465^{+0.000027}_{-0.000029}$
T_P	Time of Periastron (BJD$_{\rm TDB}$)	$2455071.37^{+0.20}_{-0.19}$
T_S	Time of eclipse (BJD$_{\rm TDB}$)	2454750 ± 110
Wavelength Parameters:		*Kepler*
u_1	linear limb-darkening coefficient	0.454 ± 0.039
u_2	quadratic limb-darkening coefficient	0.264 ± 0.049
Telescope Parameters:		Keck-HIRES
$\gamma_{\rm rel}$	Relative RV Offset^c (m/s)	$33.9^{+3.4}_{-3.6}$
σ_J	RV Jitter (m s^{-1})	$6.7^{+4.4}_{-4.2}$

See Table 3 in Eastman et al. (2019) for a detailed description of all parameters and all default (non-informative) priors.

[a] $\omega_\star$ is the argument of periastron of the star's orbit due to the planet.

[b] Calculated with Equation 3, which assumes no albedo and perfect redistribution. Between apastron and periastron, $T_{\rm eq}$ varies from 180–900 K. See the text for a discussion.

[c] Reference epoch is BJD$_{\rm TDB}$ = 2457429.435011

2020). Following the astrometric solution of Lindegren et al. (2020)[7], we subtracted -0.026 ± 0.013 mas from the EDR3 value.

For the SED portion of the EXOFASTv2 fit, we modeled broadband photometry from 2MASS (Cutri et al. 2003), ALLWISE (Cutri & et al. 2014), and Gaia (Gaia Collaboration et al. 2018) with inflated uncertainties as recommended by Eastman et al. (2019). In doing so, we employed the MIST stellar evolution models (Paxton et al. 2011, 2013, 2015; Dotter 2016; Choi et al. 2016) packaged within EXOFASTv2. We imposed a noise floor of 2% on the bolometric flux used in the SED modeling following Tayar et al. (2020).

The EXOFASTv2 fit progressed until the number of independent draws of the underlying posterior probability distribution of each parameter exceeded 1000 and the Gelman–Rubin statistic for each parameter decreased below 1.01 (Gelman & Rubin 1992; Ford 2006). We show the resulting best fit models with the transit and RV data in Figures 5 and 6, respectively.

3.1. *The Bimodality of Stellar Mass and Age*

The converged EXOFASTv2 fit yielded bimodal posterior probability distributions for the stellar mass ($M_\star$) and age (Figure 7). The region of parameter space preferred by the MIST stellar evolution models, as influenced by all of the KOI-375 data, exists near the subgiant branch as we suspected based on the SpecMatch radius estimation. EXOFASTv2 found that multiple stellar ages and surface gravity values ($\log g$) correspond to the $T_{\rm eff}$ prior, meaning that the bimodality is astrophysical and not due to inadequate poste-

[7] We calculated the astrometric solution using the software described at https://www.cosmos.esa.int/web/gaia/edr3-code.

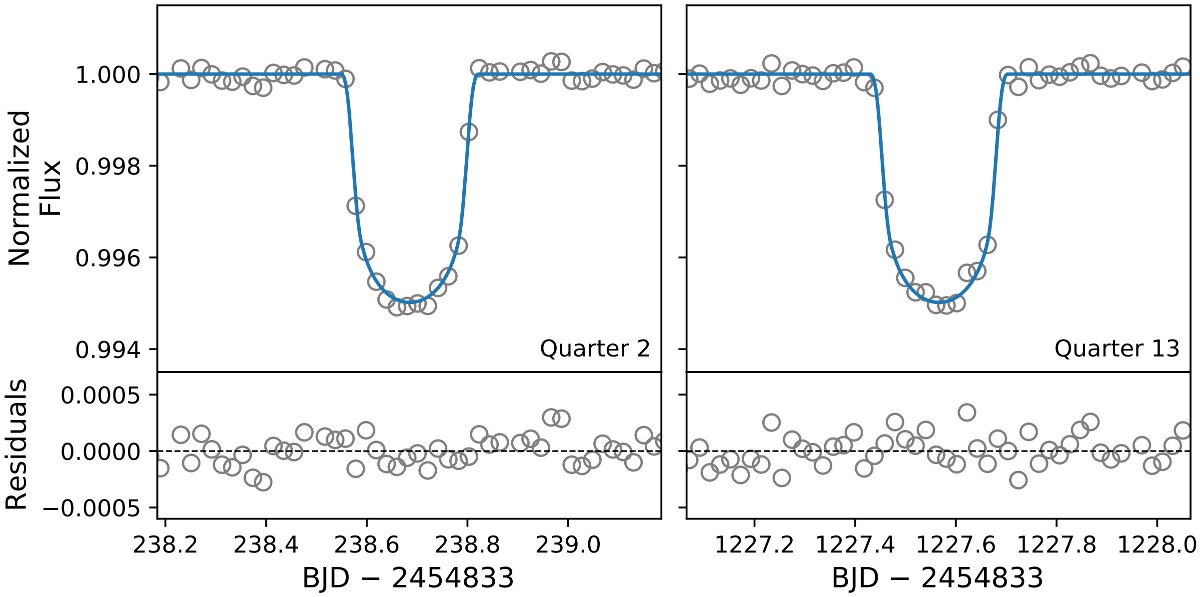

Figure 5. Detrended *Kepler* photometry of both transits (gray circles) and the best fit EXOFASTv2 model (blue line) laid over.

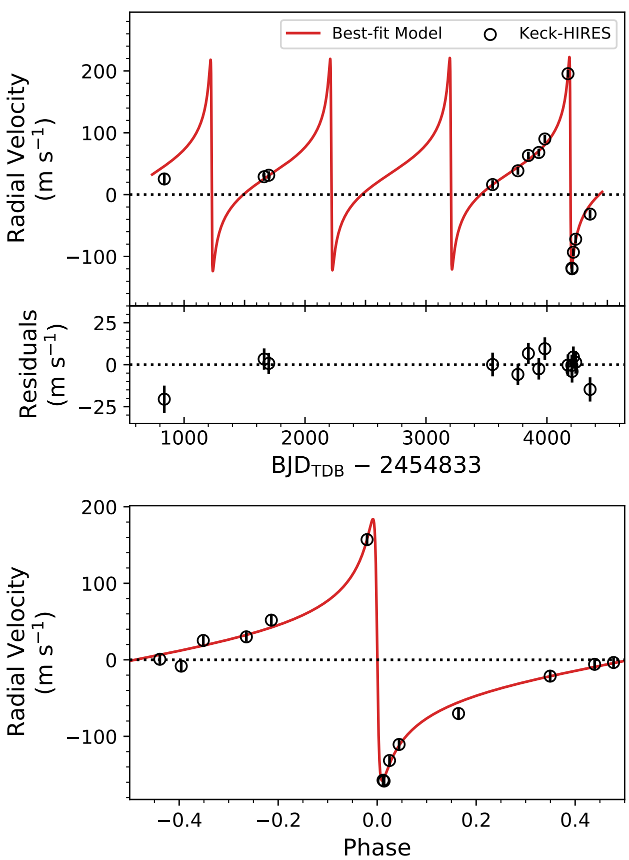

Figure 6. RV measurements of KOI-375 from Keck-HIRES with the best fit EXOFASTv2 model. The top panel shows the time series RVs and the bottom panel shows the data phase-folded on the best-fit ephemeris with $P = 988.88$ days.

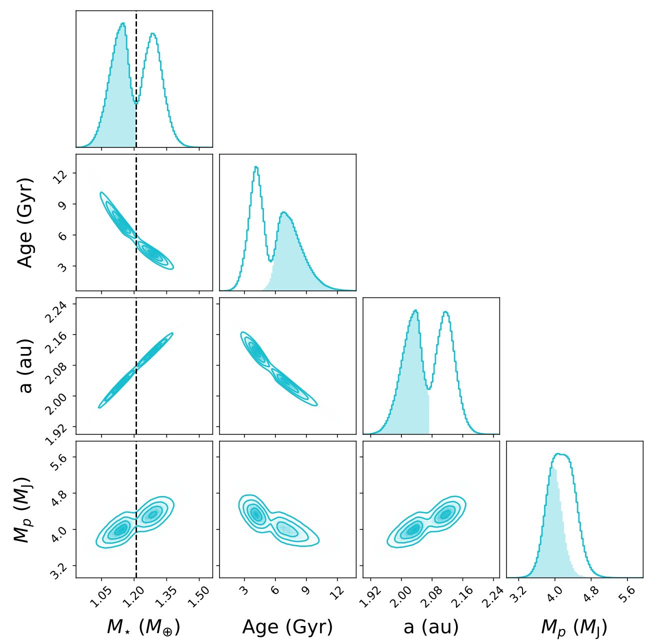

Figure 7. Posterior probability distributions demonstrating the bimodality in stellar properties and its effect on the inferred properties of KOI-375.01. The dashed vertical line at 1.21 $M_\odot$ shows where we separated the low and high mass solutions, the former of which is slightly preferred (51.8% to 48.2%) and is shown as the shaded portion of each distribution.

rior sampling. The bimodality propagates to the semi-major axis (a) of KOI-375.01 and, to a lesser extent, its mass (M_p; Figure 7).

Since we could not distinguish between the two families of solutions with the data of the KOI-375 system in hand, we adopted the strategy of Ikwut-Ukwa et al. (2020) and divided the solutions at a fiducial $M_\star$ value of 1.21 $M_\odot$, which corresponds to the trough between the posterior probability peaks in Figure 7. The lower stellar mass, older age solution contains 51.8% of the posterior samples, which we treated as a slight preference over the higher stellar mass, younger solution. Therefore, in Tables 2 and 3, we only publish the parameters for preferred, lower stellar mass solution. With the exception of a and M_p, which differ between the two solutions by 2.7σ and 1.4σ, respectively, no other planetary parameters show significant variation. None of the interpretations of the nature or formation history of KOI-375.01 are changed by considering the alternate solution.

4. RESULTS

4.1. *Confirming KOI-375.01 as a Genuine Planet*

A photometric dimming event with a depth corresponding to a giant planet transit can easily be created by substellar or stellar objects or various systematic signals (e.g., Brown 2003; Torres et al. 2005; Cameron 2012; Foreman-Mackey et al. 2016; Dalba et al. 2020a). These false positive signals can be harder to identify for longer (compared to shorter) periods owing to the difficulty in quantifying the reliability of genuine transit events from similarly long-period exoplanets (e.g., Thompson et al. 2018). Indeed, Santerne et al. (2016) measured a 55% false-positive rate for *Kepler* giant planets within 400 days of orbital period. For these reasons, long-period giant planet candidates like KOI-375.01 must be vetted with Doppler spectroscopy before any weight is placed upon their standing as a genuine planet.

Our 10-year baseline of RV measurements for KOI-375, although modest in size, confirmed the genuine planetary nature of KOI-375.01. It also confirmed the 988.88 day orbital period, placing KOI-375.01 among the top five longest-period (non-controversial) transiting exoplanets with precisely measured periods known to date[8]. With a semi-major axis of 2.03 au and an orbital eccentricity of 0.92, its elongated orbit brings it within 0.16 au of its host star and then slingshots it out to 3.9 au—the longest apastron distance of any transiting exoplanet with known orbital period and eccentricity. Figure 8 is a diagram showing the orbit of KOI-375.01 relative to those of Jupiter, the Solar System terrestrial planets, and HD 80606 b. The RV data also contain a slight, although tentative, acceleration ($0.0031^{+0.0029}_{-0.0027}$ m s^{-1} day^{-1}) that possibly indicates the existence of an outer companion.

The equilibrium temperature ($T_{\rm eq}$) for KOI-375.01 as shown in Table 3 is calculated following

$$T_{\rm eq} = T_{\rm eff}\sqrt{\frac{R_\star}{2a}}\,, \tag{3}$$

[8] According to the NASA Exoplanet Archive, accessed 2021 February 4.

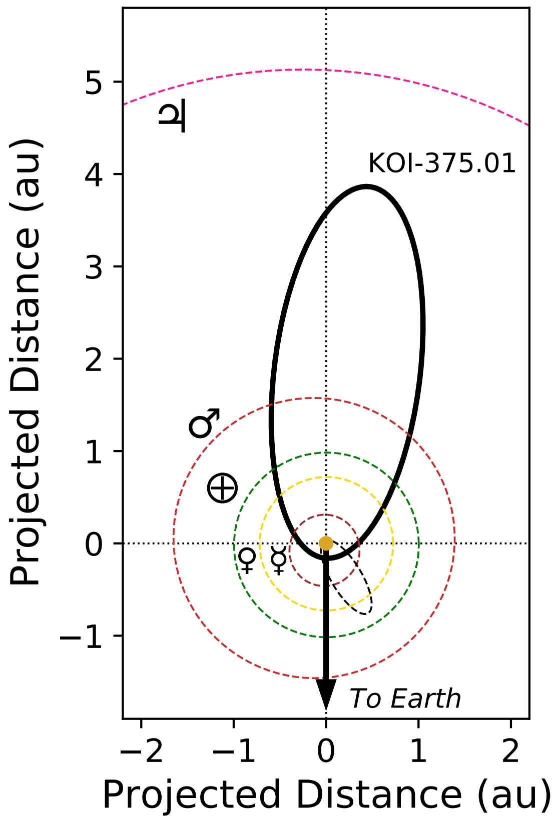

Figure 8. Face-on view of the orbit of KOI-375.01. The orbits of five Solar System planets and HD 80606 b (dashed black line) are included for reference. All orbits are drawn to scale, although the size of KOI-375 is not.

which assumes no albedo and perfect heat redistribution (Hansen & Barman 2007). However, including a factor of $1/(\sqrt{1\pm e})$ in this equation suggests that $T_{\rm eq}$ varies from $\sim$180 K at apastron to $\sim$900 K at periastron. This substantial $\sim$700 K swing in temperature likely affects the atmosphere on KOI-375.01.

In the following sections, we will investigate the possibility of companions, migration history, interior composition, and atmospheric characterization prospects for KOI-375.01. We take advantage of the fact that this planet's orbital period, eccentricity, and radius are known precisely, which is remarkable for an exoplanet with its orbital properties.

4.2. *Outer Companions in the KOI-375 System*

As described in Section 1 and extensively in the broader orbital dynamics literature (e.g., Naoz 2016), the presence of an outer planetary or stellar companion may have direct consequences on the migration history of a giant planet. For KOI-375, archival AO imaging data yield a non-detection of stellar companions beyond $\sim$100 au and upper mass limits on such a companion down to $\sim$50 au (see Figure 4 and Section 2.3). In the following sections, we exploit our long-baseline of RV observations to improve upon these limits with an injection-recovery test (Section 4.2.1), a RV trend analysis (Section 4.2.2), and a chaos indicator analysis (Section 4.2.3).

4.2.1. *RV Injection-Recovery Test*

We characterized the sensitivity of our RV data set to additional bound companions by running injection-recovery tests, in which we added synthetic signals to our RV data and converted the signal recovery rate into a map of search completeness. We used RVSearch (Rosenthal et al. 2021, accepted), an iterative periodogram search algorithm, to search for evidence of additional companions to KOI-375.01 in the RV data and perform these tests. We initialized RVSearch with the best-fit Keplerian model for KOI-375.01 and searched for additional companions with orbital periods spanning 2–10000 days. We found no evidence for additional companions in this period range. Once the search was completed, RVSearch injected synthetic planets into the data and repeated the additional iteration to determine whether it recovered these synthetic planets. We ran 3000 injection tests for KOI-375. We drew the injected planet semi-major axis and $M_p \sin i$ from log-uniform distributions, and drew eccentricity from the Beta distribution with shape parameters $\alpha = 0.867$ and $\beta = 3.03$, which Kipping (2013a) found represented the sample of RV-observed exoplanets. After RVSearch performed the injection-recovery tests, we measured search completeness across a wide range of semi-major axis and $M_p \sin i$ by determining the fraction of recovered synthetic signals in localized regions of a and $M_p \sin i$.

Figure 9 shows a pair of search completeness results, one of which includes the first low-S/N RV data point (left panel) and one of which neglects it (right panel). In both cases, our RV sensitivity to companions beyond the orbital separation of KOI-375.01 is limited, dropping below 50% completeness at 4 M_J beyond 4 au. The sparsity and high RMS of the RV data set drive the high lower limit on detectability in $M_p \sin i$, and the nearly 10-year observational baseline sets the sharp change in completeness around 3 au.

4.2.2. *RV Trend Analysis*

To build upon the injection-recovery test, we conducted a complementary test of the Keck-HIRES RVs specifically focused on evidence of acceleration (i.e., a long-term RV trend). This analysis focused specifically on partially sampled signals from giant planets, substellar object, or stars that could be lurking undetected in the outer reaches of the KOI-375 system. When combined with a nondetection from high-contrast imaging, RV trends have been shown to greatly reduce the parameter space that a possible undetected companion could occupy (e.g., Crepp et al. 2012; Kane et al. 2019; Dalba et al. 2020b)

The EXOFASTv2 fit (Section 3) to the transit, RV, and SED included a parameter for "RV slope" ($\dot{\gamma}$), which quantifies any acceleration measured from the RVs. As shown in Table 3, we made a low significance detection of acceleration as $\dot{\gamma} = 0.0031^{+0.0029}_{-0.0027}$ m s^{-1} day^{-1}. To refine the mass (M_c) and orbital distance (a_c) of the companion that could have caused this RV drift, we simulated RVs over a grid of scenarios broadly following the procedure of Montet et al. (2014).

First, we subtracted the maximum likelihood EXOFASTv2 solution for KOI-375.01 from the Keck-HIRES RV data but without including the acceleration (i.e., we set $\dot{\gamma} = 0$). In doing so, we also inflated the RV uncertainties ($\sigma_{v_r}(t)$) to account for the fitted RV jitter (Table 3). The resulting RV time series ($v_r(t)$) then only contained the long-term trend.

Next, we defined a logarithmically spaced 30x30 grid in companion mass (1 $M_J < M_c <$ 1 $M_\odot$) and semi-major axis ($4 < a/\text{au} < 200$). The mass boundaries were chosen to complement the constraints from the injection-recovery tests (Section 4.2.1) and the AO imaging (Section 2.3). The orbital distance boundaries were chosen to span the gap between the apastron distance of KOI-375.01 and the stringent upper boundary from the AO imaging.

At each point along the M_c–a_c grid, we drew 500 sets of the orbital elements [ω, e, i], which are the argument of periastron, the eccentricity, and the inclination, respectively. We drew ω randomly from a uniform distribution over the interval [0, 2π], and we drew i randomly from a uniform distribution in $\cos i$ over the interval [0, 1]. For e, we drew values from the Beta distribution from Kipping (2013b) mentioned previously (Section 4.2.1). These random draws were meant to account for the variety of orbital configurations a massive companion could have.

Then, for each of the individual orbits, we simulated 50 sets of RV time series ($\hat{v}_r(t)$) with a cadence matching v_r. Each of the 50 sets started at a different orbital phase spaced evenly across the entire orbit. This accounted for the fact that the Keck-HIRES observations could have sampled any portion of the companion's orbit.

Finally, we used a least-squares regression routine to minimize the familiar statistic $\chi^2 = \sum_t [v_r(t) - \hat{v}_r(t)]^2 / \sigma_{v_r}(t)^2$. This minimization was necessary because the Keck-HIRES RVs are relative, not absolute. Assuming uncorrelated errors, we converted the 50 χ^2 values for each individual orbit to relative probabilities following $P \propto \exp(-\chi^2/2)$, and we summed the probabilities to effectively marginalize over the portion of the orbit captured by the data. We also summed the probabilities of the 500 sets of orbits at each grid point to effectively marginalize over all orbital properties other than M_c and a_c. Lastly, we normalized the map of probabilities such that 22.5 million probability calculations summed to unity. Figure 10 (left panel) shows the resulting map.

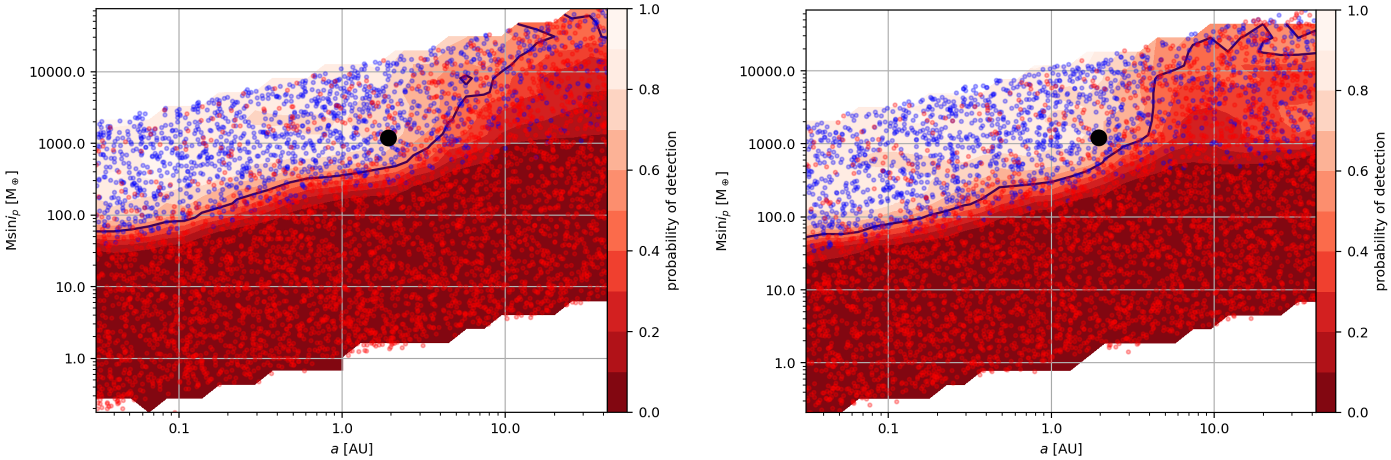

Figure 9. RVSearch injection and recovery to search for other signals in the RV data set. The left panel shows completeness contours for all RV data, while the right panel shows contours with the earliest RV data point removed (see Section 2.2). Red dots represent injected signals that were not recovered as opposed to blue dots that show recovered signals. The black dot is KOI-375.01, and the black line shows the 50% recovery contour.

The slight acceleration detected in the full set of RVs prefers companions within roughly 30 au and less massive than a few hundred Jupiter masses. However, only the most massive companions considered ($M_c \gtrsim 700\ M_J$) are confidently ruled out between 4 and 200 au in the left panel of Figure 10. Also, incorporating the upper mass limit from the AO imaging (Section 2.3) trims a small portion of parameter space, notably for a correlated region at the highest masses and largest orbital separations.

We also repeated this entire analysis but after removing the first Keck-HIRES RV data point, as its timing and quality may have inaccurately affected the measured RV trend (Section 2.2). The resulting map of probabilities calculated without the first RV data point is shown in the right panel of Figure 10. For context supporting the second probability map, we conducted a second EXOFASTv2 fit without the first Keck-HIRES data point that was otherwise identical to the fit described in Section 3. The only appreciable difference between the two EXOFASTv2 fits was value of $\dot{\gamma}$, which decreased in significance to -0.0002 ± 0.0029 m s^{-1} day^{-1} in the latter case. This difference manifests in the probability map as a much stronger constraint on M_c for $a_c < 20$ au. Although the RV baseline was shorter, and therefore less sensitive to subtle trends, the $\sim$7-year baseline of RVs was remarkably flat and confidently ($\geq 3\sigma$) excludes most companions interior to 20 au and more massive than a few hundred Jupiter masses. This limit is complemented by the AO imaging upper limit, which excludes an otherwise viable region of moderate-to-high-mass, wide separation companions. Trends in probability in Figure 10 broadly follow those in the injection-recovery analysis (Figure 9, right panel), despite extending to much higher masses than were sampled in the latter case.

4.2.3. *MEGNO Simulations*

To test whether additional constraints can be put on the orbital configurations of the potential outer companion, we ran a dynamical simulation using the Mean Exponential Growth of Nearby Orbits (MEGNO) chaos indicator (Cincotta & Simó 2000). The MEGNO indicator demonstrates whether a specific system configuration would lead to chaos after a certain integration time by distinguishing between quasi-periodic and chaotic evolution of the bodies within the system (e.g., Hinse et al. 2010). The final MEGNO value returned for a specific orbital configuration is useful for determining the stochasticity of the configuration, where chaos is more likely to result in unstable orbits for planetary bodies. With a grid of orbital parameters, a MEGNO simulation can provide valuable information on the orbital configurations that are favored by dynamical simulations, and reject configurations that return chaos results.

The MEGNO simulation to explore the dynamically viable locations for various outer companions was carried out within the N-body package REBOUND (Rein & Liu 2012) with the symplectic integrator WHFast (Rein & Tamayo 2015). We used the stellar and planetary parameters from Table 2 and Table 3, respectively. We provided a linear-uniform grid in semi-major axis (20–60 au) and companion mass (1–100 M_J) that aligned with the higher probability region in Figure 10 (right panel). The eccentricity of the outer companion was set to zero. The simulation was integrated for 20 million years with a time step of 0.034 years ($\sim$12.4 days). This time step was chosen to be 1/80 of the orbital period of KOI-375.01, a fourth of the recommended value (Duncan et al. 1998), to increase the sampling near the periastron passage of this highly eccentric planet. The integration was set

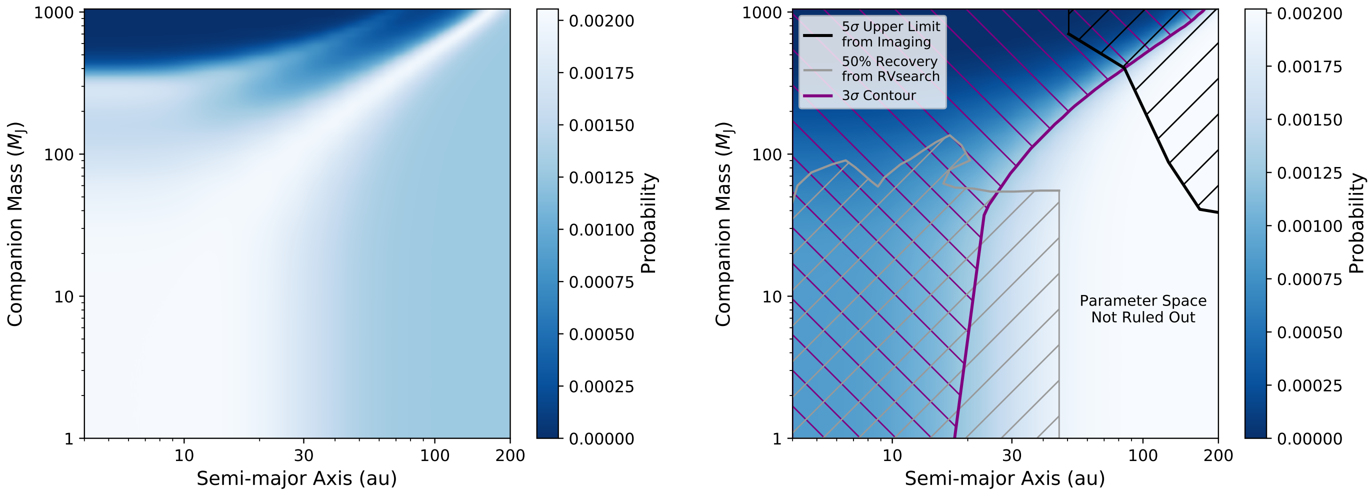

Figure 10. Probability of a companion in mass and semi-major axis space based on the expected acceleration relative to the residuals in the Keck-HIRES RVs after the signal from KOI-375.01 was subtracted. *Left:* Probabilities were calculated using all Keck-HIRES RV data points. *Right:* Probabilities were calculated after removing the first Keck-HIRES RV data point (Section 2.2. The black hatched region is ruled out to 5σ by the AO imaging (Figure 4). The purple line is drawn at $P = 0.0013$ such that the hatched area is ruled out to greater than 3σ. Any potential candidates in the gray hatched region have greater than a 50% recovery rate (Figure 9, right panel).

to stop and return chaos results if any of the planetary orbits started extending beyond 100 au.

Figure 11 shows the grid of results of the MEGNO simulation. Each grid point is color coded according to the final MEGNO value for the orbital configuration of that outer companion. A MEGNO value around 2 (green) is considered non-chaotic (Hinse et al. 2010) and are thus dynamically viable regions where the outer companion could exist without making the system chaotic. Grid points in red indicate simulations that returned chaotic results, and those in white indicate irregular events such as close encounters and collisions, all of which are unfavorable configurations for an outer companion.

Only a few small pockets of parameter space (lower semi-major axes, higher masses) contain orbital configurations that lead to chaos. Otherwise, this analysis fails to rule out any extra substantial area of parameter space where a massive companion could exist.

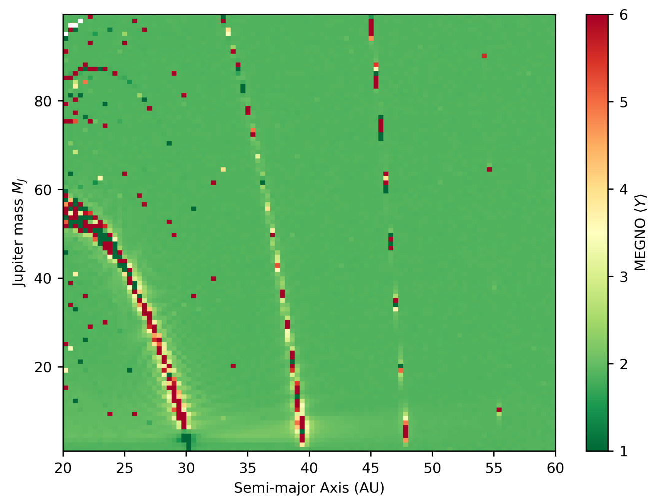

Figure 11. MEGNO simulation result with a grid of orbital configurations for the outer companion. Green regions (low values) are stable against chaos.

4.3. *Bulk Metallicity Retrieval for KOI-375.01*

Continuing our discussion of results, we now shift the attention from the outer reaches of the KOI-375 system back to KOI-375.01 itself.

With the measured mass and radius of KOI-375.01, along with other system properties, we retrieved the mass of its heavy elements or its bulk metals (M_z) and calculated its bulk metallicity ($Z_p \equiv M_z/M_p$) following Thorngren & Fortney (2019). Briefly, we modeled the thermal evolution of KOI-375.01 using one-dimensional structure models with a core composed of a rock–ice mixture at equal amounts, a homogeneous convective envelope made of a H/He–rock–ice mixture, and a radiative atmosphere. The atmosphere models were interpolated from the grid of Fortney et al. (2007). Samples were drawn from the posterior probability distributions for planet mass, radius, and age (Section 3), and the heavy element mass was adjusted in the structure models to recover the planet radius.

This analysis relied on two assumptions. First, we assumed that the planet radius is not inflated (e.g., Laughlin 2018) because the average irradiation flux received by KOI-375.01 (see Table 3), which is well below the canonical 2×10^8 erg s^{-1} cm^{-2} empirical threshold for giant planets (Miller & Fortney 2011; Demory & Seager 2011; Sestovic

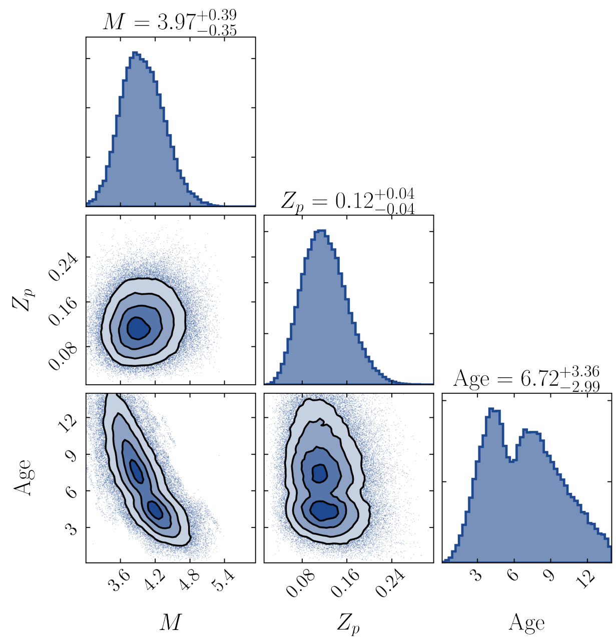

Figure 12. Posterior probability distributions from the heavy element mass retrieval for KOI-375.01. The symbols M and Z_p represent planet mass and bulk metallicity, respectively. Despite the bimodality in age (see Section 3), Z_p is normal. The inferred bulk metallicity of KOI-375.01 corresponds to a heavy element mass of $\sim$150 $M_\oplus$ and an enrichment (relative to stellar) of $\sim$5.

et al. 2018). Second, we neglected any internal heating from circularization tides. We assumed that tides are an inefficient means of heating KOI-375.01 as evidenced by the 80000 Gyr tidal circularization timescale (Table 3).

The metallicity retrieval was complicated slightly by the bimodal probability distribution for age we inferred from the comprehensive system modeling (Figure 7). Instead of using separate normal priors for stellar mass and age, we used a bivariate Gaussian kernel-density estimate as the prior for these parameters. Then, we sampled the posterior with a Markov chain Monte Carlo technique.

The results of the bulk metal mass retrieval are shown in Figure 12. Despite the bimodality in age, the marginalized posterior probability distribution for bulk metallicity is a near-normal distribution at $Z_p = 0.12 \pm 0.04$, corresponding to $M_z \approx 150\ M_\oplus$. To calculate the stellar metallicity ($Z_\star$), we assumed that the iron abundance ([Fe/H]) scales with total heavy metal content such that $Z_\star \equiv 0.0142 \times 10^{[\mathrm{Fe/H}]}$ (Asplund et al. 2009; Miller & Fortney 2011), which yields $Z_\star = 0.0229 \pm 0.0031$. Finally, we calculated the bulk metallicity enrichment relative to stellar for KOI-375.01 as $Z_p/Z_\star = 5.2 \pm 1.9$.

We place the bulk metal mass and metallicity enrichment in context of other cool ($T_{\mathrm{eq}} \lesssim 1000$ K), weakly irradiated ($\langle F \rangle < 2 \times 10^8$ erg s^{-1} cm^{-2}) giant exoplanets from the Thorngren et al. (2016) sample[9] in Figure 13. By metal mass and enrichment, KOI-375.01 is entirely consistent with the known trends. KOI-375.01 contains more metal mass than its lower-mass counterparts, but it is broadly less enriched in metals relative to its host star. These findings support the theory of core accretion as its formation scenario, followed by a period of late-stage heavy element accretion (e.g., Mousis et al. 2009; Mordasini et al. 2014). KOI-375.01 is similar to the other high-mass ($M_p \gtrsim 2\ M_\mathrm{J}$) giant planets in that it orbits a metal-rich star, something that has been predicted by population synthesis models (e.g., Mordasini et al. 2012) and likely relates to the correlation between host star metallicity and giant planet occurrence (e.g., Gonzalez 1997; Santos et al. 2004; Fischer & Valenti 2005).

In Figure 13 (right panel), we include a prediction from Ginzburg & Chiang (2020), who model concurrent gas accretion and mergers in giant planet formation. The scatter in the data enclosed by the dotted black lines can be explained by the intrinsically chaotic nature of mergers, even if all systems evolve from nearly identical conditions as quantified by an average critical core mass of 10 $M_\oplus$. The majority of the credible interval for the metallicity enrichment of KOI-375.01 falls outside of this theoretical range. However, Ginzburg & Chiang (2020) demonstrated that loosening the constraint on the average core mass needed to begin runaway gas accretion to 3–30 $M_\oplus$ can account for all of the scatter measured by Thorngren et al. (2016) as well as KOI-375.01.

It is interesting to consider how trends in heavy element mass, metal enrichment, and total planet mass relate to other orbital and stellar properties. In Figure 14, we show the relative residuals (calculated/best fit) of heavy element mass and metallicity enrichment (relative to stellar) as a function of eccentricity for the Thorngren et al. (2016) sample of weakly irradiated giant exoplanets and KOI-375.01. As noted by Thorngren et al. (2016), there is no discernible trend in either quantity. However, given how sparsely populated the high-eccentricity region is, it is worthwhile to consider the (now) five individual systems with $e > 0.6$. The residual heavy element mass and metallicity enrichment of KOI-375.01 and HD 80606 b are nearly identical, as are their orbital eccentricity and planet mass. However, as we will discuss in Section 5, HD 80606 b likely migrated via secular perturbations with HD 80607 (e.g., Wu & Murray 2003; Fabrycky & Tremaine 2007; Winn et al. 2009) whereas we have largely ruled out a stellar companion for KOI-375. If KOI-375.01 and HD 80606 b followed different migration pathways, there is no evidence in their bulk metallicity to distinguish them. Oddly, the residual heavy element mass and the

[9] We exclude Kepler-75 b in all related figures and analyses since Thorngren et al. (2016) only derived an upper limit on its metal mass.

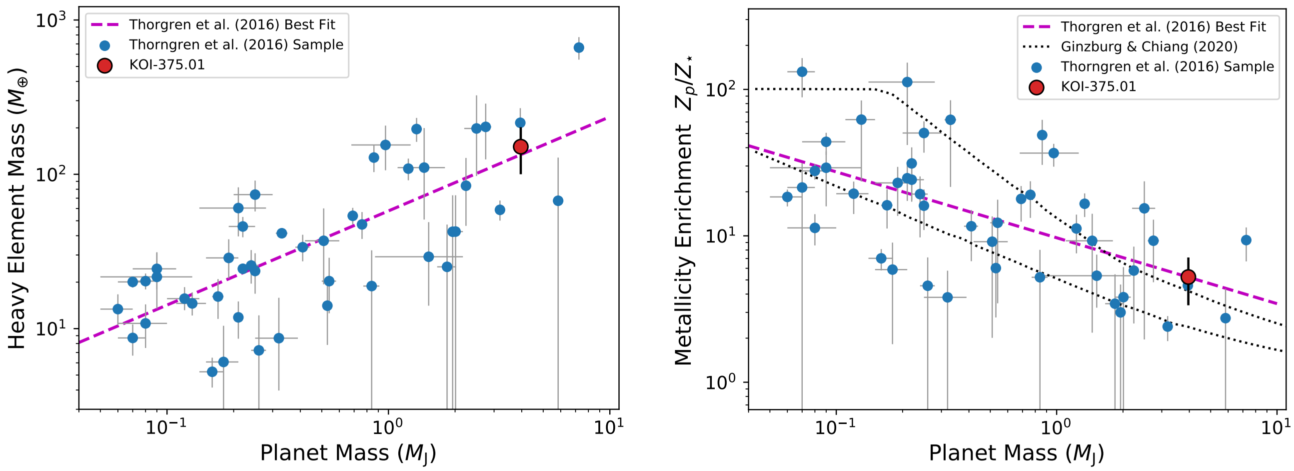

Figure 13. *Left:* Heavy element mass of the weakly irradiated giant exoplanets from Thorngren et al. (2016) as well as KOI-375.01. *Right:* Metallicity enrichment of the weakly irradiated giant exoplanets from Thorngren et al. (2016) as well as KOI-375.01. The dotted black lines show the scatter that can be accounted for by concurrent gas accretion and mergers assuming an average core mass of 10 $M_\oplus$ at the onset of runaway gas accretion (Ginzburg & Chiang 2020). The position of KOI-375.01 in these panels suggests a formation by core accretion with substantial late stage accretion of heavy elements.

metallicity enrichment of these two planets are significantly different than those of HD 17156 b, which has $e \approx 0.67$ (Fischer et al. 2007; Bonomo et al. 2017). However, unlike HD 80606 b, HD 17156 b has no stellar companion and its orbit is nearly aligned with its host star (Cochran et al. 2008; Narita et al. 2008; Barbieri et al. 2009). Also, HD 17156 b's orbital period is almost two orders of magnitude shorter than that of KOI-375.01. Therefore, it is perhaps not surprising that these planets experienced different formation histories that could account for the metallicity differences. The final two high-eccentricity planets in Figure 14 (KOI-1257 b and Kepler-419 b) have relatively imprecise residual heavy element masses and metallicity enrichments. KOI-1257 b is thought to be in a binary star system, possibly pointing to Kozai migration (Santerne et al. 2014). On the other hand, Kepler-419 b is joined by a massive outer giant planet that has a low mutual inclination, such that Kozai migration is likely not a viable migration theory (Dawson et al. 2014). The overall lack of a clear trend between heavy element mass or metallicity enrichment and the presence of a companion and/or high stellar obliquity is likely in part a result of the small number of data points. However, it could also suggest that the heavy element accretion occurs before or independently from the various HEM channels.

4.4. *Atmospheric Characterization Prospects for KOI-375.01*

The bulk heavy element mass retrieval suggested that ∼150 Earth-masses of metals should exist within KOI-375.01. Assuming a core mass of ∼10 $M_\oplus$, or even up to 30 $M_\oplus$ as may be suggested by Figure 13, this yields a prediction of a metal-enriched gaseous envelope like Jupiter

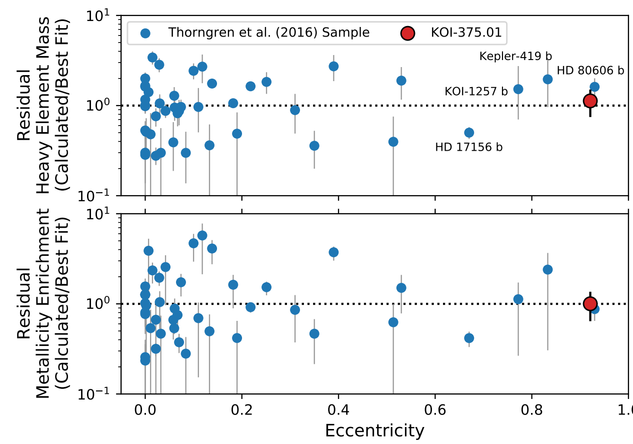

Figure 14. Relative residuals (calculated/best fit) of heavy element mass (top) and metallicity enrichment relative to stellar (bottom) as a function of eccentricity for the Thorngren et al. (2016) sample of weakly irradiated giant exoplanets and KOI-375.01.

(e.g., Wong et al. 2004) or Saturn (Fletcher et al. 2009b) that could possibly be explored via atmospheric characterization. Specifically, Thorngren & Fortney (2019) showed that the bulk metallicity places an upper limit on the atmospheric metallicity. For KOI-375.01, the core-free 2σ upper limit ($Z_p = 0.2$) for atmospheric metallicity is 35.7× solar.

Considering only orbital period or semi-major axis, KOI-375.01 is a rare opportunity for transmission spectroscopy (Seager & Sasselov 2000). Although, long-period exoplanets pose specific challenges to this kind of technique. Not only are transits of such planets geometrically rare, but their timing is often uncertain. Since only two transits of KOI-375.01 have been observed, the presence of extreme transit timing variations (TTVs; Wang et al. 2015b) cannot be ruled out (e.g., Dalba & Muirhead 2016; Dalba & Tamburo 2019). Furthermore, atmospheric temperature will (to first order) decrease with increasing orbital distance. As a result, atmospheres will be cooler and scale heights and transmission spectrum features will be smaller. Surprisingly, this can be balanced by low surface gravity, as would be the case if Saturn was subject to transmission spectroscopy (Dalba et al. 2015). The transiting geometry of the long-period KOI-375.01 also makes it a unique candidate for testing theories of atmospheric refraction (e.g., Sidis & Sari 2010; Dalba 2017; Alp & Demory 2018) that have not yet been observationally tested (Sheets et al. 2018).

However, considering the large radius of the subgiant KOI-375 and the high mass of KOI-375.01, this system is a challenging target for transmission spectroscopy. With a surface gravity of 86 m s^{-2} and the average equilibrium temperature of 254 K from Table 3, the atmospheric scale height is only $\sim$12 km, which corresponds to 1 part-per-million (ppm) in the transmission spectrum. The out-of-transit stellar mirage caused by refraction also scales with the atmospheric scale height (e.g., Dalba 2017), making such a detection similarly difficult.

On the other hand, we used Equation 3 to estimate that $T_{\rm eq}$ at periastron, which is within several days of transit, is $\sim$900 K. This suggests a 3.6$\times$ increase in the atmospheric scale height and transmission spectrum feature size. Although 4 ppm is still beyond the reach of current and future facilities, we caution that our intuition for predicting favorable transmission spectroscopy targets is largely based on our current understanding of hot, close-in exoplanet atmospheres. This possibly warrants skepticism. After all, Saturn—as a transiting exoplanet—would be surprisingly amenable to transmission spectroscopy (Dalba et al. 2015). Other long-period giant exoplanets may prove surprising as well.

Even if transmission spectroscopy is not a viable atmospheric characterization technique, the 0.16 au periastron distance of KOI-375.01 caused by its extreme eccentricity possible qualifies it for an IR phase curve analysis.

4.4.1. *IR Phase Curve Analysis*

To predict the expected thermal signature of the planet during periastron passage, we calculated the IR phase curve for KOI-375.01 during one complete orbital period. These calculations followed the methodology of Kane & Gelino (2011) using the stellar and planetary parameters provided in Tables 2 and 3, respectively. We assumed a passband of 4.5 μm, a Bond albedo of zero, and we calculated the flux ratio of planet to star using the "hot dayside" and "well mixed" models.

These models represent the extremes of heat redistributions as they assume re-radiated energy over 2π and 4π sr, respectively. The full IR phase curve for both models are shown in Figure 15, along with a zoomed panel that shows the location of the periastron passage.

There are several caveats to this calculation. We assumed an instantaneous response of the planetary absorption and IR emission, whereas the radiative and advective time scales will determine the nature of phase lags in thermal emission profiles (Langton & Laughlin 2008; Cowan & Agol 2011a). This, combined with the blackbody emission and zero albedo assumptions, means that the calculations presented in Figure 15 may be considered as an upper limit on the expected IR emission. Furthermore, the variation in temperature would also alter the atmospheric composition. Some of the energy would be converted into latent heat to dissociate larger molecules or particulates. There would also be an interconversion between CO and CH_4 (e.g., Visscher 2012). The timescale of this reaction, and also the vertical mixing timescale, should be considered to produce a more accurate model of the phase curve. We leave these considerations for a future work and instead derive a first-order, upper limit on the phase curve emission.

Despite the various assumptions that apply to this phase curve modeling, the order of magnitude ($\mathcal{O}(10^2)$ ppm) of the thermal flux increase is likely accurate. Several instruments on board the *JWST* will have sensitivity in the near- to thermal-IR and, based on preliminary noise floor expectations (Greene et al. 2016), should be capable of detecting the KOI-375.01 phase variation. Borrowing from solar system intuition, 4–6 μm is likely a promising wavelength for such an observation. Ignoring clouds, Jupiter and Saturn's atmospheres have low opacity in this wavelength region that exists between bands of methane and phosphine where radiation from 5–8 bars can escape (Irwin et al. 2014). Jupiter's radiance near 5 μm even exceeds that at mid-IR wavelengths (e.g., Irwin et al. 1998; Fletcher et al. 2009a; Irwin et al. 2014).

The periastron passage of KOI-375.01 is spread over $\sim$10 days and includes the transit. Low cadence time series observations from the F444W filter of NIRCam, for example, could detect the peak flux ratio and the width of the feature assuming that the visit-to-visit photometric stability does not overwhelm the astrophysical signal. Including at least one high cadence, longer visit at or following periastron would also be valuable because the phase curve may exhibit a "ringing" as the hot spot from periastron rotates in and out of view (e.g., Cowan & Agol 2011b). This effect is not featured in our simulation of KOI-375.01, which assumed pseudo-synchronous rotation. However, given the inefficiency of tides at the periastron distance of KOI-375.01, this assumption may be an oversimplification. The detection of a ringing oscillation in the phase would test this assump-

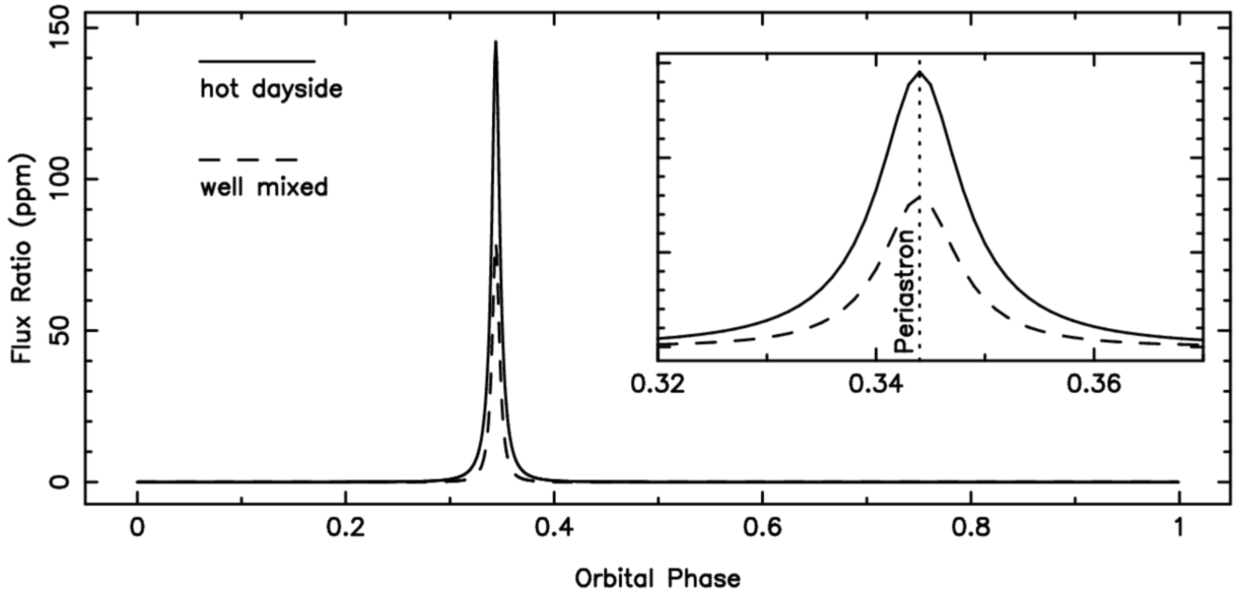

Figure 15. Simulated 4.5 μm phase curve of KOI-375.01 following Kane & Gelino (2011). The "hot dayside" and "well mixed" models correspond to atmospheric heat redistribution efficiencies of 0 and 1, respectively. The $\sim$100 ppm amplitude of this variation is favorable for *JWST* observation. This simulation assumed a pseudo-synchronous rotation of KOI-375.01. If the planet's rotation is not synchronized, an oscillation in flux at the frequency of the planets effective rotation rate may also be detectable.

tion and possibly directly yield the effective planetary rotation rate.

A full simulation of the detectability of the thermal phase curve for KOI-375.01 is beyond the scope of this paper and should likely wait until *JWST* is launched and commissioned. In addition to a broad band detection of phase variability, the prospects for spectroscopic detection should also be investigated. It seems unlikely that transmission spectroscopy will be an effective tool to measure atmospheric composition (e.g., metallicity), so any any other possible method would be extremely useful. Atmospheric metal enrichment (relative to stellar) is a specifically valuable property to measure because it can be compared to the planet's bulk metallicity enhancement (Section 4.3). One prediction would be an atmospheric metallicity less than the bulk metallicity if some heavy elements comprise a planetary core or there is otherwise an increasing gradient in metals with depth. Even a rough estimation of core properties would be useful for our prediction of a core mass up to $\sim$30 $M_\oplus$ based on Ginzburg & Chiang (2020) as described in Section 4.3. However, recent high-precision gravity data and well established atmospheric composition results suggest a more complicated picture for Jupiter and Saturn (Niemann et al. 1998; Wong et al. 2004; Fletcher et al. 2009b; Wahl et al. 2017; Guillot et al. 2018; Iess et al. 2019; Müller et al. 2020b). More elaborate theories include inverse compositional gradients (e.g., Debras & Chabrier 2019) are needed to explain Jupiter and Saturn and could possibly be refined through atmospheric characterization of exoplanets like KOI-375.01.

Based on the optimistic prospect of *JWST* observations, we determined the timing of transits and periastron passages of KOI-375.01 occurring in the next 10 years (Table 4). For each event, we checked for visibility from *JWST* using the General Target Visibility Tool[10] This tool only predicts visibility through the end of 2023, but we assumed the same visibility of KOI-375 in all later years. The 2023 transit of KOI-375.01 will not be visible to *JWST* while the 2028 transit will be. The 2025 transit will occur within 24 hr after the visibility window closes and the 2031 transit will occur roughly six days after the visibility window opens. If the solar avoidance restrictions change after launch, these transits may or may not be visible to *JWST*. The periastron passage of KOI-375.01 occurs several hours before transit, so its visibility is similar. However, as shown in Figure 15, the peak of the thermal flux ratio spans $\sim$10 days. Even if the exact moment of periastron is (or is not visible), some portion of the event is expected to be visible to *JWST*.

4.4.2. *Radio Emission*

Unlike for transmission spectroscopy, the relatively high mass of KOI-375.01 is beneficial to attempts to measure planetary radio emission. Lazio et al. (2010) searched for radio emission from HD 80606 b during a periastron passage but measured only an upper limit. That experiment was based on the expectation that the variation in planet–star distance over an eccentric orbit would lead to dramatic increase in

[10] Accessed 2021 February 11 (https://github.com/spacetelescope/jwst_gtvt).

Table 4. Future Transit and Periastron Timing Predictions

	Conjunction (Transit) Time		Periastron Time		*JWST*
Epoch[a]	BJD_{TDB}	UTC	BJD_{TDB}	UTC	Visibility[b]
5	2460016.0902 ± 0.0021	2023-03-12 14:10	2460015.78 ± 0.20	2023-03-12 06:37	None
6	2461004.9714 ± 0.0023	2025-11-25 11:19	2461004.66 ± 0.20	2025-11-25 03:46	Partial
7	2461993.8525 ± 0.0025	2028-08-10 08:28	2461993.54 ± 0.20	2028-08-10 00:55	Full
8	2462982.7336 ± 0.0027	2031-04-26 05:36	2462982.42 ± 0.20	2031-04-25 22:03	Partial

[a] Epoch=0 is defined as the first transit observed by the *Kepler* spacecraft.

[b] *JWST* visibility after 2023 December 31 is based on previous years' visibility. Epochs for which the full periastron passage of KOI-375.01 partially falls outside of the predicted visibility windows are labeled as "Partial" (see the text).

magnetospheric emission. Assuming that luminosity scales with the planet–star distance as $L \propto d^{-1.6}$ (e.g., Farrell et al. 1999), then the factor of 24.3 change in distance would produce a 165x increase in luminosity. While this is slightly smaller than the 200x increase expected for HD 80606 b, a future radio search may be aided by the fact that KOI-375.01 can possibly emit at higher frequencies. We estimate that the upper limit emission frequency as determined by the local plasma frequency in the emission region for KOI-375.01 is

$$\nu = 24\ \mathrm{MHz} \left(\frac{\omega}{\omega_J}\right) \left(\frac{M_p}{M_J}\right)^{5/3} \left(\frac{R_p}{R_J}\right)^{3} \quad (4)$$

where ω is the angular rotation rate (Farrell et al. 1999; Lazio et al. 2004, 2010). In this Equation, all values are scaled to those of Jupiter. For HD 80606 b, tidal forces are expected to force the planet into pseudo-synchronous rotation (Hut 1981; Lazio et al. 2010), with a rotation period of 39.9 hr. It is unlikely that this would also apply to KOI-375.01, for which the larger periastron distance renders tides inefficient. Therefore, the assumption of a Jupiter-like rotation period ($\sim$9.9 hr) is reasonable. In that case, evaluating Equation 4 gives 287 MHz. Lazio et al. (2010) argued that this equation may actually under-predict the cutoff frequency of exoplanets, as it does for Jupiter, and suggested that the upper limit may be 60% larger. In that case, the cutoff frequency for KOI-375.01 would be 406 MHz, which is more accessible to existing radio observatories than HD 80606 b's 55–90 MHz.

A full simulation of the potential for radio emission from KOI-375.01 is beyond the scope of this paper, and the ability to make such a detection, at least relative to previous attempts for HD 80606 b, will likely be hindered somewhat by the greater distance to the KOI-375 system. However, even the admittedly coarse calculation here suggests that KOI-375.01 is one of the best systems to investigate magnetospheric response to a rapidly changing planet–star distance. Such an observation stands to extend the study of giant exoplanet magnetic fields beyond the inner most hot Jupiters (e.g., Cauley et al. 2019) and explore magnetic field generation in planets akin to Jupiter and Saturn.

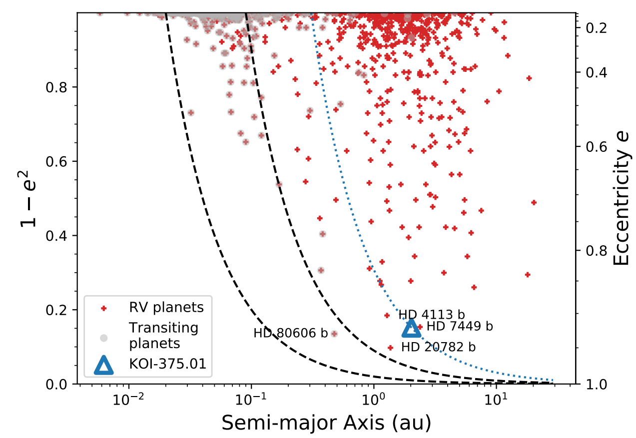

Figure 16. The eccentricity for all non-controversial exoplanets with known a (or with the necessary parameters to calculate a) and with (minimum) mass greater than 0.3 M_J as listed in the NASA Exoplanet Archive (accessed 2021 February 17). The marker indicates whether a planet has been detected by transits and/or RVs. The dashed black lines indicate tracks of constant angular momentum with final orbital periods of 1 and 10 days. The dotted blue line indicates the track for KOI-375.01.

5. DISCUSSION

Much of the previous analysis has focused on key pieces of information that inform the formation and migration history of KOI-375.01. Orbital period and eccentricity are two of the most notable properties in this respect. As shown in Figure 16, these properties place KOI-375.01 among a small group of known exoplanets on long-period, highly eccentric orbits that are useful for testing the extremes of planetary formation theories. More remarkable, though, is the transiting geometry of the orbit of KOI-375.01. Relative to other transiting exoplanets, the position of KOI-375.01 in a–e space is unrivaled (Figure 16). KOI-375.01 thereby offers its radius and bulk composition, as well as its orbital properties, a clues to its formation and migration history.

Here, we attempt to assemble all of these pieces of information into a coherent narrative describing the history of this interesting planet.

5.1. *KOI-375.01: The Failed Hot Jupiter*

Based solely on the measured orbital eccentricity, we discard disk-migration as the explanation for the orbital properties of KOI-375.01. Papaloizou et al. (2001) showed that eccentricities up to ∼0.25 could be achieved through disk interactions for a variety of planet masses. Although, eccentricity is generally damped by the disk for giant planets with $M_p < 5\ M_J$ (Bitsch et al. 2013). Recent work revisiting disk cavity migration argued for eccentricities up to 0.4 for giant planets (Debras et al. 2021), which is possibly a viable theory for other outer giant planets like Kepler-1514 b ($e = 0.401$), which also harbors an inner Earth-sized companion (Dalba et al. 2021). Explaining the eccentricity of KOI-375.01, however, requires HEM.

Through multiple analyses, we ruled out planetary, substellar, and stellar companions in the KOI-375 system across a broad parameter space. Unknown stellar companions (with masses in the range 50–400 $M_\odot$) are limited to a narrow range of semi-major axis between 20 and 150 au (Figure 10, right panel). Unknown substellar and planetary companions are limited to semi-major axes above ∼45 au. Companions within these parameter spaces (and the otherwise ruled out spaces) could have driven KOI-375.01 to its high eccentricity through secular Kozai–Lidov perturbations (e.g., Wu & Murray 2003; Naoz et al. 2011). Also, star-planet Kozai migration from a stellar companion that was present when KOI-375.01 formed but subsequently lost due three-body interactions also remains a possible explanation. However, motivated by our non-detection of a companion and only a tentative detection of acceleration in ∼10 years of RV measurements, we discard secular perturbations as being the most likely explanation for the high eccentricity of KOI-375.01 given the information in hand.

We recommend future that dynamical simulations explore the specific area of parameter space to see if an additional hidden companion could theoretically be responsible for the properties of KOI-375.01 (c.f., Jackson et al. 2019).

This brings us to HEM theories involving close, fast dynamical interactions. Specifically, could planet-planet scattering (e.g., Rasio & Ford 1996) provide an explanation for the eccentricity of KOI-375.01? Many aspects of the observed eccentricity distribution of giant exoplanets can be explained by planet-planet scattering (e.g., Moorhead & Adams 2005; Chatterjee et al. 2008; Raymond et al. 2010; Bitsch et al. 2020), including planets with eccentricities above 0.99 (Carrera et al. 2019). For KOI-375.01, we find planet-planet scattering is consistent with its orbital properties, its host stars, and its bulk interior properties. KOI-375 is a metal-rich star ([Fe/H] = 0.196 ± 0.057 from Table 2). Dawson & Murray-Clay (2013) demonstrated that metal-rich stars tend to host high-eccentricity hot Jupiters, which they interpreted as evidence support HEM by planet-planet scattering owing to the well know correlation between stellar metallicity and giant planet occurrence (e.g., Santos et al. 2004; Fischer & Valenti 2005). Even though KOI-375.01 is not a hot Jupiter it is reasonable that it could have formed alongside other giant planets that were subsequently scattered. After many close encounters, possibly even tens of thousands (Carrera et al. 2019), KOI-375.01 could have been driven to its current eccentricity. It is at this point that its path may deviated from that of hot Jupiter. Hot Jupiters tend to have some type of companion that might explain their migration history (e.g., Bryan et al. 2016), whereas we have not detected a companion for KOI-375.01. We speculate that KOI-375.01 either merged with or ejected the companions that would have continued driving its eccentricity. At that point, its final periastron distance was too far for tides to efficiently circularize the orbit (the tidal circularization timescale is far longer than the age of the universe). Even given that time, tidal migration (at constant angular momentum) would only reduce the orbital period to ∼59 days (Figure 16). This leaves KOI-375.01 as the failed hot Jupiter that we have characterized here. This hypothesis yields a prediction that highly eccentric *failed* hot Jupiter planets like KOI-375.01 will be alone in their systems. Kepler-419 b is perhaps a noteworthy exception to this prediction, although disk migration may have been in play for that system (Petrovich et al. 2019).

The bulk heavy element mass of KOI-375.01 (∼150 $M_\oplus$) is consistent with theories suggesting that the accretion of metals occurred concurrently with migration via scattering. Shibata et al. (2020) found that migration during gas accretion allows giant planets to capture tens of Earths masses worth of planetesimals that would not be available *in situ*. The amount of heavy elements scales with increasing migration distance and decreasing migration timescale, both of which are expected for HEM through planet-planet scattering. Furthermore, the simulations of Ginzburg & Chiang (2020) offer some evidence that the critical core mass of KOI-375.01 might be greater than the 10 $M_\oplus$ required to efficiently accrete gas (e.g., Pollack et al. 1996). One way of overcoming this is through the coagulation of protoplanetary embryos undergoing type-I migration prior to the dispersal of the protostellar disk (Liu et al. 2015). These protoplanetary embryos themselves may even scatter each other to higher eccentricities. Bitsch et al. (2020) found that scattering events are common and more embryos lead to giant planets with higher eccentricities so long as the damping rates for inclination and eccentricity are slow. Indeed slow rates are required to reproduce the eccentricity distribution of the known giant planets (Bitsch et al. 2020).

A subtle but important point in this discussion is that planet mergers (or collisions) are less efficient at producing high eccentricities than scattering events (e.g., Ford & Rasio 2008; Jurić & Tremaine 2008; Anderson et al. 2020). As a result, we suspect that mergers and scattering events, possibly occurring at similar times, both played important roles in the formation of KOI-375.01.

All of these theories and the lack of an outer companion point to a consistent picture of the migration that began before the dispersal of the disk whereby mergers, close encounters, and scattering events delivered KOI-375.01 to its current orbit with its current bulk composition. Moving forward, it would be useful to compare this outcome to other well characterized outer transiting giant planets. It will be particularly interesting to compare the bulk interior properties of giant planets in systems with and without outer companions that could have induced Kozai migration. If bulk heavy element composition and migration mechanisms are linked, as seems to be the case for KOI-375.01, we might expect to find a correlation between interior properties and the existence of companions.

A critical missing piece in our discussion of the migration of KOI-375.01 is the stellar obliquity. A substantially misaligned orbit of KOI-375.01 would warrant a reexamination of Kozai migration, although planet-planet scattering can also cause misaligned orbits (e.g., Naoz et al. 2012). Moreover, the effective temperature of KOI-375 ($\sim$5750 K) makes this system a perfect laboratory for testing the theory that hot Jupiters preferentially realign cool stars (e.g., Winn et al. 2010; Schlaufman 2010). The effective temperature of KOI-375 is 5745^{+88}_{-89} K, which is well below the $\sim$6200 K Kraft break (Kraft 1967) that has been implicated by hot Jupiter obliquity observations. Since tidal forces are inefficient for failed hot Jupiters like KOI-375.01, we would expect that these planets would show a variety of obliquities and would not be preferentially aligned like hot Jupiters orbiting similarly cool stars.

In theory, the obliquity between KOI-375.01 and its host star could be measured through the Rossiter–McLaughlin (RM) effect (Rossiter 1924; McLaughlin 1924). If successful, it would stand as the longest-period planet, by far, to have an obliquity measurement. In practice, an RM experiment will be challenging. Our SpecMatch analysis (Section 2.2) inferred a low stellar rotational velocity of 2.74 ± 1.0 km s^{-1}. By Equation 40 of Winn (2010), the maximum expected amplitude of the RM effect is only 11 m s^{-1}. Assuming 30 minute exposure times (as used for the current RV data), this would only allow 12 data points across the entire transit. With the $\sim$7 m s^{-1} RV precision achieved using the best-match template (see Table 1 and Section 2.2), any detection of obliquity would likely be marginal. We recommend that any future effort to observe the spectroscopic transit of KOI-375.01 should first acquire a high-S/N spectral template of KOI-375 to reduce the internal RV precision by several m s^{-1}. Owing to the extreme eccentricity and the argument of periastron, the transit duration is short enough that a fortunately timed transit could be observed from a single site. For the Keck I telescope, only the second half of the 2023 transit (Table 4) is visible. KOI-375 will rise above the Nasmyth deck at Keck I at a favorable airmass of $\sim$1.5 around 14:30 UTC on 2023 March 12. Again assuming 30 minute exposure times, that would place roughly 6 data points across the second half of RM signal. Even with the actual template and improved internal precision, a detection of obliquity would likely be moderate at best. It is not until 2028 that the Keck I telescope has the optimal position for an RM detection. The mid-transit time of the August 2028 transit is almost perfect timed with KOI-375 crossing the meridian, and the full transit (plus post-transit baseline) is observable. However, in the coming years, new precise RV facilities with the capability of achieving few m s^{-1} precision on faint (V = 13.4) stars such as MAROON-X (Seifahrt et al. 2018) or the Keck Planet Finder (Gibson et al. 2016) should consider conducting RM measurements of long-period *Kepler* planets like KOI-375.01.

KOI-375 represents an interesting comparison for the Kepler-167 system, in which an early K dwarf star hosts three inner super-Earth-sized planets and an outer transiting Jupiter-analog on a P = 1071 day orbit (Kipping et al. 2016). Although the mass of Kepler-167 e—the outer giant planet—has not been measured yet, its orbital eccentricity has been constrained to $\sim$ 0.06 by the transit shape and duration. This low eccentricity combined with the presence of multiple inner super-Earth planets suggests that the migration mechanism for Kepler-167 e was likely gentle and driven by interactions with the disk. Kepler-167 is solar metallicity, if not slightly metal poor, so it is possible that Kepler-167 e was only giant planet formed in the outer disk, so scattering events never occurred. Dalba & Tamburo (2019) ruled out the existence of TTVs in the ephemeris of Kepler-167 e, which further implies a lack of an outer massive companion. A mass and bulk metallicity measurement for Kepler-167 e would provide an interesting comparison with KOI-375.01, which likely experienced dynamical interactions with other bodies during and/or after its formation.

5.2. *Could KOI-375.01 Host Exomoons?*

Giant transiting exoplanets with multi-year orbital periods are possibly exciting targets for dedicated exomoons searches (e.g., Kipping et al. 2012a; Heller et al. 2014; Teachey & Kipping 2018). Now that we have measured the mass and orbital properties of KOI-375.01, the plausibility of this planet hosting a system of exomoons should be investigated in more detail. Given the suspected active dynamical formation history of KOI-375.01, its ability to have maintained a system of exomoons is perhaps questionable. Indeed, the investigation of exomoon stability under tidal forces (e.g., Barnes & O'Brien 2002; Adams & Bloch 2016; Sucerquia et al. 2020), planet-planet scattering (e.g., Nesvorný et al. 2007; Gong et al. 2013; Hong et al. 2018), disk torques (e.g., Namouni 2010; Spalding et al. 2016), and secular migration owing to a stellar companion (e.g., Martinez et al. 2019; Trani et al. 2020) are active areas of theoretical research. Although any such studies is beyond the scope of this work, we can approximate the Hill radius of KOI-375.01 at periastron (where it is smallest):

$$r_{\rm H,peri} \approx a(1-e)\left(\frac{M_p}{3M_\star}\right)^{1/3} . \quad (5)$$

For KOI-375.01, we find that $r_{\rm H,peri} \approx 2.5 \times 10^6$ km. This calculation suggests that any exomoon orbiting KOI-375.01 would need a semi-major axis less than this value to survive the close periastron passages. For perspective, the semi-major axis of Callisto, Jupiter's most distant Galilean moon, is roughly 1.9×10^6 km. Of course, this calculation neglects all of the processes that led to KOI-375.01 reaching its current orbital configuration, which is likely imprudent. We offer KOI-375.01 as a potentially interesting case study for more detailed investigations of exomoon formation and stability in the future.

The fact that KOI-375.01 swings through its host star's habitable zone on its eccentric orbit is also potentially interesting from an exomoon standpoint (e.g., Heller 2012; Heller & Barnes 2013; Hill et al. 2018). However, the plausibility of life developing on an exomoon that experiences such intense variation in stellar irradiation ought to be thoroughly scrutinized.

5.3. *One Path Forward for Giant Outer Transiting Exoplanets*

The vast majority of known giant planets on au-scale orbits have unknown radii because they either do not transit or they are not known to transit. Without a radius, subsequent investigations of atmospheres and interiors are uncertain if not altogether impossible. Measuring the masses of the modest sample of known transiting giant planets with au-scale orbits and discovering more such planets will be important to advancing our understanding of giant planet formation and migration. These discoveries will also drive new theoretical advances in giant planet interiors, which are needed given that changing model assumptions can substantially alter our conclusions about the interior structures of giant exoplanets (e.g., Müller et al. 2020a).

Only a handful of outer giant exoplanets like KOI-375.01 exist within the *Kepler* sample and they all orbit relatively faint stars. This creates two problems. Firstly, their limited number means that unfortunate transit timing (see Table 4 and also Dalba & Tamburo (2019)) can drastically slow progress to obtain new observations and advance our theoretical understanding. Secondly, their faintness must be overcome (if at all possible) by larger investments of highly competitive telescope time.

The Transiting Exoplanet Survey Satellite (TESS; Ricker et al. 2015), which is actively searching for transits of bright stars around the entire sky, presents solutions to both problems. The only drawback is the tendency of TESS's observing strategy to yield single transit events for most planets with orbital periods greater than a couple dozen days (e.g., Gill et al. 2020; Dalba et al. 2020c; Díaz et al. 2020; Lendl et al. 2020). If the *Kepler* mission had adopted the TESS mission's observing strategy, not only would KOI-375.01 have been identified through a single transit, but its 6 hr transit duration could have easily been misconstrued as corresponding to a relatively short ($\sim$15 days) orbital period. This suggests (and more quantitative efforts have shown; Cooke et al. 2018; Villanueva et al. 2019) that given enough time and targets, TESS will identify transits from a unprecedented sample of long-period giant planets. Yet, the advancement of giant planet theory and understanding will rely on continued challenging follow-up efforts to characterize these planets masses, orbits, interiors, and atmospheres.

6. SUMMARY

We obtained nearly 10 years of RV observations of the $\sim$ 5750 K subgiant star KOI-375, which was found to host a transiting giant planet candidate (KOI-375.01) by the primary *Kepler* mission. Our observations and analyses confirmed the genuine nature of this exoplanet, now known as KOI-375.01, which is a 4.0-Jupiter-mass planet on a 988.88 day orbit with an extreme $0.921^{+0.010}_{-0.015}$ eccentricity. We included AO imaging analysis, interior and atmosphere modeling, and dynamical simulations to characterize this system and make predictions for future observations. The primary results of this work are as follows.

1. We collected 14 RV measurements (Table 1) of KOI-375 from Keck-HIRES spanning 9.6 years that confirm the 988.88 day orbital period for KOI-375.01, thereby ruling out the possibility of a third transit occurring in a *Kepler* data gap (Section 2.1). The RVs also confirmed the extremely high orbital eccentricity ($e = 0.921^{+0.010}_{-0.015}$) that was suspected from the photoeccentric effect modeling (Section 2.1.1) and measured the planet mass to be $3.96^{+0.20}_{-0.19}$ $M_{\rm J}$. KOI-375.01 has the longest apastron distance (3.9 au) of any confirmed transiting exoplanet with a precisely known orbital period. Moreover, we found that between periastron and apastron, the equilibrium temperature of KOI-375.01 varies from $\sim$180 K to $\sim$900 K.

2. Archival AO imaging of KOI-375 from the PHARO instrument identified three possible stellar companions within $\sim$10″, two of which were previously published (Wang et al. 2015a). We found that two of the companions are spurious sources and the third is not gravitationally associated (Section 2.3). Additional archival AO imaging from the NIRC2 instrument (Furlan et al. 2017) yielded a non-detection of stellar companions within 2″ and placed upper limits on the mass of any undetected companion within 1000 au of KOI-375 (Figure 4).

3. The joint analysis of transit, RV, and broadband photometry (Section 3) identified a bimodality in stellar properties due to the evolutionary state of KOI-375 (Figure 7). We split the solutions based on stellar mass and publish the favored set of stellar and planetary parameters in Tables 2 and 3, respectively.

4. We conducted three investigations of companions to KOI-375.01 (Section 4.2). Firstly, an injection-recovery analysis demonstrated that the RVs of KOI-375 are sensitive enough to have detected planetary companions within the orbit of KOI-375.01 down to $\sim$100 $M_\oplus$ and companions out to a few au with a few Jupiter masses (Figure 9). Secondly, we synthesized RV time series to determine the region of mass–semimajor-axis parameter space that is consistent with the subtle acceleration of KOI-375, leaving only the possibility of companions less than a few hundred Jupiter-masses and beyond $\sim$45 au (Figure 10, right panel). Thirdly, we conducted a dynamical simulation using the MEGNO chaos indicator that failed to substantially rule out any other regions of parameter space for additional companions (Figure 11). Based on these three analyses, we disfavor, although fail to entirely rule out, Kozai migration and secular chaos as the likely scenario to explain the orbital properties of KOI-375.01.

5. Using the mass and radius of KOI-375.01 and the bimodal age of KOI-375, we retrieved the bulk heavy element mass (and metal enrichment relative to stellar) for KOI-375.01 (Figure 12). This planet likely contains $\sim$150 $M_\oplus$ of heavy elements, making it enriched relative to KOI-375 by a factor of $\sim$5. These finding suggest that KOI-375.01 is consistent with the mass–metallicity trends of Thorngren et al. (2016) and theories of core accretion with late-stage heavy element accretion (Figure 13). However, the metal enrichment also suggests that KOI-375.01 may have experienced planetesimal mergers during formation that increased its critical core mass above 10 $M_\oplus$ (Section 4.3).

6. Based on the aforementioned analyses, we hypothesized that KOI-375.01 is a failed hot Jupiter (e.g., Dawson et al. 2014) that reached its high eccentricity through planet-planet scattering events, but its periastron distance was too large for efficient tidal circularization (Section 5.1). We speculate that it may have ejected the companions needed to continue driving up its eccentricity, yielding the prediction that most failed hot Jupiters will be alone. The stellar metallicity of KOI-375 and the bulk composition of KOI-375.01 are consistent with theories of mergers, scattering events, and migration during the gas accretion phase of its formation.

7. A critical missing piece of the discussion on the migration of KOI-375.01, however, is the stellar obliquity (Section 5.1). Given the 5750 K effective temperature of KOI-375, this system can provide a rare and valuable test of the hot Jupiter formation theory that hot Jupiter preferentially align the spins of cool stars (e.g., Winn et al. 2010). A detection of the RM effect for this system is feasible, however the timing of the future transits of KOI-375.01 (Table 4) will make this a challenging endeavour.

8. Finally, we consider prospects for characterizing the atmosphere of KOI-375.01 (Section 4.4.1). While the large stellar radius and high planet mass will largely impede transmission spectroscopy, the IR phase curve of KOI-375.01 near periastron is expected to be detectable from *JWST* (Figure 15). Such a detection would reveal the heat redistribution properties of this cold ($T_{\rm eq}$ = 254 K) Jovian planet. Furthermore, since tidal forces are inefficient, the rotation of KOI-375.01 is likely not pseudo-synchronized with its orbit, and its rotation period is possibly detectable as a "ringing" in thermal phase curve (e.g., Cowan & Agol 2011b).

The GOT 'EM survey aims to characterize systems of long-period transiting giant planets, which serve as stepping stones between many exoplanet systems and the solar system (Dalba et al. 2021). KOI-375.01 is an extraordinary system owing to its high eccentricity and transiting geometry. Much like HD 80606 b, KOI-375.01 provides a laboratory for testing the extremes of planetary migration scenarios. Continued observation and characterization of this system stands to refine the theories underlying the formation and evolution of all planetary systems.

ACKNOWLEDGMENTS

The authors thank all of the observers in the California Planet Search team for their many hours of hard work. The authors thank Ji Wang for a helpful discussion about PHARO AO imaging. The authors thank all of the members of the Unistellar Citizen Science campaign to observe KOI-375. P. D. is supported by a National Science Foundation (NSF) Astronomy and Astrophysics Postdoctoral Fellowship under award AST-1903811. E. W. S. acknowledges support from the NASA Astrobiology Institute's Alternative Earths team funded under Cooperative Agreement Number NNA15BB03A and the Virtual Planetary Laboratory, which is a member of the NASA Nexus for Exoplanet System Science, and funded via NASA Astrobiology Program Grant No. 80NSSC18K0829.

This research has made use of the NASA Exoplanet Archive, which is operated by the California Institute of Technology, under contract with the National Aeronautics and Space Administration under the Exoplanet Exploration Program. This paper includes data collected by the *Kepler* mission and obtained from the MAST data archive at the Space Telescope Science Institute (STScI). Funding for the Kepler mission is provided by the NASA Science Mission Directorate. STScI is operated by the Association of Universities for Research in Astronomy, Inc., under NASA contract NAS 5–26555. This research has made use of the Exoplanet Follow-up Observation Program website, which is operated by the California Institute of Technology, under contract with the National Aeronautics and Space Administration under the Exoplanet Exploration Program.

Some of the data presented herein were obtained at the W. M. Keck Observatory, which is operated as a scientific partnership among the California Institute of Technology, the University of California, and NASA. The Observatory was made possible by the generous financial support of the W. M. Keck Foundation. Some of the Keck data were obtained under PI Data awards 2013A and 2013B (M. Payne). Finally, the authors recognize and acknowledge the cultural role and reverence that the summit of Maunakea has within the indigenous Hawaiian community. We are deeply grateful to have the opportunity to conduct observations from this mountain.

Facilities: Keck:I (HIRES), Keck:II (NIRC2), Kepler, Hale (PHARO)

Software: astropy (Astropy Collaboration et al. 2013, 2018), corner (Foreman-Mackey 2016), EXOFASTv2 (Eastman et al. 2013; Eastman 2017; Eastman et al. 2019), lightkurve (Lightkurve Collaboration et al. 2018), SpecMatch (Petigura 2015; Petigura et al. 2017), `SpecMatch-Emp` (Yee et al. 2017), exoplanet (Foreman-Mackey et al. 2020), pymc3 (Salvatier et al. 2016), theano (Theano Development Team 2016), REBOUND (Rein & Liu 2012), RVSearch (Rosenthal et al. 2021, accepted)

REFERENCES

Adams, F. C., & Bloch, A. M. 2016, MNRAS, 462, 2527, doi: 10.1093/mnras/stw1883

Alibert, Y., Mousis, O., Mordasini, C., & Benz, W. 2005, ApJL, 626, L57, doi: 10.1086/431325

Alp, D., & Demory, B. O. 2018, A&A, 609, A90, doi: 10.1051/0004-6361/201731484

Anderson, K. R., Lai, D., & Pu, B. 2020, MNRAS, 491, 1369, doi: 10.1093/mnras/stz3119

Asplund, M., Grevesse, N., Sauval, A. J., & Scott, P. 2009, ARA&A, 47, 481, doi: 10.1146/annurev.astro.46.060407.145222

Astropy Collaboration, Robitaille, T. P., Tollerud, E. J., et al. 2013, A&A, 558, A33, doi: 10.1051/0004-6361/201322068

Astropy Collaboration, Price-Whelan, A. M., Sipőcz, B. M., et al. 2018, AJ, 156, 123, doi: 10.3847/1538-3881/aabc4f

Baraffe, I., Chabrier, G., Barman, T. S., Allard, F., & Hauschildt, P. H. 2003, A&A, 402, 701, doi: 10.1051/0004-6361:20030252

Barbieri, M., Alonso, R., Desidera, S., et al. 2009, A&A, 503, 601, doi: 10.1051/0004-6361/200811466

Barnes, J. W., & O'Brien, D. P. 2002, ApJ, 575, 1087, doi: 10.1086/341477

Baruteau, C., Crida, A., Paardekooper, S.-J., et al. 2014, in Protostars and Planets VI, ed. H. Beuther, R. S. Klessen, C. P. Dullemond, & T. Henning (Tucson: Univ. of Arizona Press), 667–689, doi: 10.2458/azu_uapress_9780816531240-ch029

Beatty, T. G., & Gaudi, B. S. 2008, ApJ, 686, 1302, doi: 10.1086/591441

Bitsch, B., Crida, A., Libert, A. S., & Lega, E. 2013, A&A, 555, A124, doi: 10.1051/0004-6361/201220310

Bitsch, B., Trifonov, T., & Izidoro, A. 2020, A&A, 643, A66, doi: 10.1051/0004-6361/202038856

Bonomo, A. S., Desidera, S., Benatti, S., et al. 2017, A&A, 602, A107, doi: 10.1051/0004-6361/201629882

Borucki, W. J., Koch, D., Basri, G., et al. 2010, Science, 327, 977, doi: 10.1126/science.1185402

Brady, M. T., Petigura, E. A., Knutson, H. A., et al. 2018, AJ, 156, 147, doi: 10.3847/1538-3881/aad773

Brown, T. M. 2003, ApJL, 593, L125, doi: 10.1086/378310

Bryan, M. L., Knutson, H. A., Howard, A. W., et al. 2016, ApJ, 821, 89, doi: 10.3847/0004-637X/821/2/89

Buchhave, L. A., Bitsch, B., Johansen, A., et al. 2018, ApJ, 856, 37, doi: 10.3847/1538-4357/aaafca

Cameron, A. C. 2012, Nature, 492, 48, doi: 10.1038/492048a

Carrera, D., Raymond, S. N., & Davies, M. B. 2019, A&A, 629, L7, doi: 10.1051/0004-6361/201935744

Cauley, P. W., Shkolnik, E. L., Llama, J., & Lanza, A. F. 2019, Nature Astronomy, 3, 1128, doi: 10.1038/s41550-019-0840-x

Chatterjee, S., Ford, E. B., Matsumura, S., & Rasio, F. A. 2008, ApJ, 686, 580, doi: 10.1086/590227

Choi, J., Dotter, A., Conroy, C., et al. 2016, ApJ, 823, 102, doi: 10.3847/0004-637X/823/2/102

Cincotta, P. M., & Simó, C. 2000, A&AS, 147, 205, doi: 10.1051/aas:2000108

Cochran, W. D., Redfield, S., Endl, M., & Cochran, A. L. 2008, ApJL, 683, L59, doi: 10.1086/591317

Cooke, B. F., Pollacco, D., West, R., McCormac, J., & Wheatley, P. J. 2018, A&A, 619, A175, doi: 10.1051/0004-6361/201834014

Cowan, N. B., & Agol, E. 2011a, ApJ, 729, 54, doi: 10.1088/0004-637X/729/1/54

—. 2011b, ApJ, 726, 82, doi: 10.1088/0004-637X/726/2/82

Crepp, J. R., Johnson, J. A., Howard, A. W., et al. 2012, ApJ, 761, 39, doi: 10.1088/0004-637X/761/1/39

Cutri, R. M., & et al. 2014, VizieR Online Data Catalog, II/328

Cutri, R. M., Skrutskie, M. F., van Dyk, S., et al. 2003, VizieR Online Data Catalog, II/246

Dalba, P. A. 2017, ApJ, 848, 91, doi: 10.3847/1538-4357/aa8e47

Dalba, P. A., Fulton, B., Isaacson, H., Kane, S. R., & Howard, A. W. 2020a, AJ, 160, 149, doi: 10.3847/1538-3881/abad27

Dalba, P. A., Kane, S. R., Barclay, T., et al. 2019, PASP, 131, 034401, doi: 10.1088/1538-3873/aaf183

Dalba, P. A., & Muirhead, P. S. 2016, ApJL, 826, L7, doi: 10.3847/2041-8205/826/1/L7

Dalba, P. A., Muirhead, P. S., Fortney, J. J., et al. 2015, ApJ, 814, 154, doi: 10.1088/0004-637X/814/2/154

Dalba, P. A., & Tamburo, P. 2019, ApJL, 873, L17, doi: 10.3847/2041-8213/ab0bb4

Dalba, P. A., Kane, S. R., Howell, S. B., et al. 2020b, arXiv e-prints, arXiv:2012.05253. https://arxiv.org/abs/2012.05253

Dalba, P. A., Gupta, A. F., Rodriguez, J. E., et al. 2020c, AJ, 159, 241, doi: 10.3847/1538-3881/ab84e3

Dalba, P. A., Kane, S. R., Isaacson, H., et al. 2021, AJ, 161, 103, doi: 10.3847/1538-3881/abd408

Dawson, R. I., & Johnson, J. A. 2012, ApJ, 756, 122, doi: 10.1088/0004-637X/756/2/122

—. 2018, ARA&A, 56, 175, doi: 10.1146/annurev-astro-081817-051853

Dawson, R. I., Johnson, J. A., Morton, T. D., et al. 2012, ApJ, 761, 163, doi: 10.1088/0004-637X/761/2/163

Dawson, R. I., & Murray-Clay, R. A. 2013, ApJL, 767, L24, doi: 10.1088/2041-8205/767/2/L24

Dawson, R. I., Murray-Clay, R. A., & Johnson, J. A. 2015, ApJ, 798, 66, doi: 10.1088/0004-637X/798/2/66

Dawson, R. I., Johnson, J. A., Fabrycky, D. C., et al. 2014, ApJ, 791, 89, doi: 10.1088/0004-637X/791/2/89

Debras, F., Baruteau, C., & Donati, J.-F. 2021, MNRAS, 500, 1621, doi: 10.1093/mnras/staa3397

Debras, F., & Chabrier, G. 2019, ApJ, 872, 100, doi: 10.3847/1538-4357/aaff65

Demory, B.-O., & Seager, S. 2011, ApJS, 197, 12, doi: 10.1088/0067-0049/197/1/12

Díaz, M. R., Jenkins, J. S., Feng, F., et al. 2020, MNRAS, 496, 4330, doi: 10.1093/mnras/staa1724

Dong, S., Katz, B., & Socrates, A. 2013, ApJL, 763, L2, doi: 10.1088/2041-8205/763/1/L2

Dotter, A. 2016, ApJS, 222, 8, doi: 10.3847/0067-0049/222/1/8

Duncan, M. J., Levison, H. F., & Lee, M. H. 1998, AJ, 116, 2067, doi: 10.1086/300541

Eastman, J. 2017, EXOFASTv2: Generalized publication-quality exoplanet modeling code, v2, Astrophysics Source Code Library. http://ascl.net/1710.003

Eastman, J., Gaudi, B. S., & Agol, E. 2013, PASP, 125, 83, doi: 10.1086/669497

Eastman, J. D., Rodriguez, J. E., Agol, E., et al. 2019, arXiv e-prints. https://arxiv.org/abs/1907.09480

Fabrycky, D., & Tremaine, S. 2007, ApJ, 669, 1298, doi: 10.1086/521702

Fabrycky, D. C., & Winn, J. N. 2009, ApJ, 696, 1230, doi: 10.1088/0004-637X/696/2/1230

Farrell, W. M., Desch, M. D., & Zarka, P. 1999, J. Geophys. Res., 104, 14025, doi: 10.1029/1998JE900050

Fischer, D. A., & Valenti, J. 2005, ApJ, 622, 1102, doi: 10.1086/428383

Fischer, D. A., Vogt, S. S., Marcy, G. W., et al. 2007, ApJ, 669, 1336, doi: 10.1086/521869

Fletcher, L. N., Orton, G. S., Teanby, N. A., & Irwin, P. G. J. 2009a, Icarus, 202, 543, doi: 10.1016/j.icarus.2009.03.023

Fletcher, L. N., Orton, G. S., Teanby, N. A., Irwin, P. G. J., & Bjoraker, G. L. 2009b, Icarus, 199, 351, doi: 10.1016/j.icarus.2008.09.019

Ford, E. B. 2006, ApJ, 642, 505, doi: 10.1086/500802

Ford, E. B., & Rasio, F. A. 2006, ApJL, 638, L45, doi: 10.1086/500734

—. 2008, ApJ, 686, 621, doi: 10.1086/590926

Foreman-Mackey, D. 2016, The Journal of Open Source Software, 24, doi: 10.21105/joss.00024

Foreman-Mackey, D., Luger, R., Czekala, I., et al. 2020, exoplanet-dev/exoplanet v0.3.2, doi: 10.5281/zenodo.1998447

Foreman-Mackey, D., Morton, T. D., Hogg, D. W., Agol, E., & Schölkopf, B. 2016, AJ, 152, 206, doi: 10.3847/0004-6256/152/6/206

Fortney, J. J., Marley, M. S., & Barnes, J. W. 2007, ApJ, 659, 1661, doi: 10.1086/512120

Furlan, E., Ciardi, D. R., Everett, M. E., et al. 2017, AJ, 153, 71, doi: 10.3847/1538-3881/153/2/71

Gaia Collaboration, Brown, A. G. A., Vallenari, A., et al. 2020, arXiv e-prints, arXiv:2012.01533. https://arxiv.org/abs/2012.01533

Gaia Collaboration, Prusti, T., de Bruijne, J. H. J., et al. 2016, A&A, 595, A1, doi: 10.1051/0004-6361/201629272

Gaia Collaboration, Brown, A. G. A., Vallenari, A., et al. 2018, A&A, 616, A1, doi: 10.1051/0004-6361/201833051

Gelman, A., & Rubin, D. B. 1992, Statistical Science, 7, 457, doi: 10.1214/ss/1177011136

Gibson, S. R., Howard, A. W., Marcy, G. W., et al. 2016, in Society of Photo-Optical Instrumentation Engineers (SPIE) Conference Series, Vol. 9908, Ground-based and Airborne Instrumentation for Astronomy VI, ed. C. J. Evans, L. Simard, & H. Takami, 990870, doi: 10.1117/12.2233334

Gill, S., Wheatley, P. J., Cooke, B. F., et al. 2020, ApJL, 898, L11, doi: 10.3847/2041-8213/ab9eb9

Ginzburg, S., & Chiang, E. 2020, MNRAS, 498, 680, doi: 10.1093/mnras/staa2500

Goldreich, P., & Tremaine, S. 1980, ApJ, 241, 425, doi: 10.1086/158356

Gong, Y.-X., Zhou, J.-L., Xie, J.-W., & Wu, X.-M. 2013, ApJL, 769, L14, doi: 10.1088/2041-8205/769/1/L14

Gonzalez, G. 1997, MNRAS, 285, 403, doi: 10.1093/mnras/285.2.403

Greene, T. P., Line, M. R., Montero, C., et al. 2016, ApJ, 817, 17, doi: 10.3847/0004-637X/817/1/17

Guillot, T., Miguel, Y., Militzer, B., et al. 2018, Nature, 555, 227, doi: 10.1038/nature25775

Hamers, A. S., Antonini, F., Lithwick, Y., Perets, H. B., & Portegies Zwart, S. F. 2017, MNRAS, 464, 688, doi: 10.1093/mnras/stw2370

Hansen, B. M. S., & Barman, T. 2007, ApJ, 671, 861, doi: 10.1086/523038

Hayward, T. L., Brandl, B., Pirger, B., et al. 2001, PASP, 113, 105, doi: 10.1086/317969

Heller, R. 2012, A&A, 545, L8, doi: 10.1051/0004-6361/201220003

Heller, R., & Barnes, R. 2013, Astrobiology, 13, 18, doi: 10.1089/ast.2012.0859

Heller, R., Williams, D., Kipping, D., et al. 2014, Astrobiology, 14, 798, doi: 10.1089/ast.2014.1147

Hill, M. L., Kane, S. R., Seperuelo Duarte, E., et al. 2018, ApJ, 860, 67, doi: 10.3847/1538-4357/aac384

Hinse, T. C., Christou, A. A., Alvarellos, J. L. A., & Goździewski, K. 2010, MNRAS, 404, 837, doi: 10.1111/j.1365-2966.2010.16307.x

Hong, Y.-C., Raymond, S. N., Nicholson, P. D., & Lunine, J. I. 2018, ApJ, 852, 85, doi: 10.3847/1538-4357/aaa0db

Howard, A. W., & Fulton, B. J. 2016, PASP, 128, 114401, doi: 10.1088/1538-3873/128/969/114401

Howard, A. W., Johnson, J. A., Marcy, G. W., et al. 2010, ApJ, 721, 1467, doi: 10.1088/0004-637X/721/2/1467

Hut, P. 1981, A&A, 99, 126

Iess, L., Militzer, B., Kaspi, Y., et al. 2019, Science, 364, aat2965, doi: 10.1126/science.aat2965

Ikwut-Ukwa, M., Rodriguez, J. E., Bieryla, A., et al. 2020, AJ, 160, 209, doi: 10.3847/1538-3881/aba964

Irwin, P. G. J., Barstow, J. K., Bowles, N. E., et al. 2014, Icarus, 242, 172, doi: 10.1016/j.icarus.2014.08.005

Irwin, P. G. J., Weir, A. L., Smith, S. E., et al. 1998, J. Geophys. Res., 103, 23001, doi: 10.1029/98JE00948

Isaacson, H., & Fischer, D. 2010, ApJ, 725, 875, doi: 10.1088/0004-637X/725/1/875

Jackson, J. M., Dawson, R. I., & Zalesky, J. 2019, AJ, 157, 166, doi: 10.3847/1538-3881/ab09eb

Jenkins, J. M., Caldwell, D. A., Chandrasekaran, H., et al. 2010, ApJL, 713, L87, doi: 10.1088/2041-8205/713/2/L87

Jurić, M., & Tremaine, S. 2008, ApJ, 686, 603, doi: 10.1086/590047

Kane, S. R. 2007, MNRAS, 380, 1488, doi: 10.1111/j.1365-2966.2007.12144.x

Kane, S. R., & Gelino, D. M. 2011, ApJ, 741, 52, doi: 10.1088/0004-637X/741/1/52

Kane, S. R., Dalba, P. A., Li, Z., et al. 2019, AJ, 157, 252, doi: 10.3847/1538-3881/ab1ddf

Kipping, D. M. 2010, MNRAS, 407, 301, doi: 10.1111/j.1365-2966.2010.16894.x

—. 2013a, MNRAS, 434, L51, doi: 10.1093/mnrasl/slt075

—. 2013b, MNRAS, 434, L51, doi: 10.1093/mnrasl/slt075

Kipping, D. M., Bakos, G. Á., Buchhave, L., Nesvorný, D., & Schmitt, A. 2012a, ApJ, 750, 115, doi: 10.1088/0004-637X/750/2/115

Kipping, D. M., Dunn, W. R., Jasinski, J. M., & Manthri, V. P. 2012b, MNRAS, 421, 1166, doi: 10.1111/j.1365-2966.2011.20376.x

Kipping, D. M., Torres, G., Henze, C., et al. 2016, ApJ, 820, 112, doi: 10.3847/0004-637X/820/2/112

Kovács, G., Zucker, S., & Mazeh, T. 2002, A&A, 391, 369, doi: 10.1051/0004-6361:20020802

Kozai, Y. 1962, AJ, 67, 591, doi: 10.1086/108790

Kraft, R. P. 1967, ApJ, 150, 551, doi: 10.1086/149359

Langton, J., & Laughlin, G. 2008, ApJ, 674, 1106, doi: 10.1086/523957

Laughlin, G. 2018, Mass-Radius Relations of Giant Planets: The Radius Anomaly and Interior Models, ed. H. J. Deeg & J. A. Belmonte (Cham: Springer), 1, doi: 10.1007/978-3-319-55333-7_1

Lazio, T. J. W., Shankland, P. D., Farrell, W. M., & Blank, D. L. 2010, AJ, 140, 1929, doi: 10.1088/0004-6256/140/6/1929

Lazio, T. Joseph, W., Farrell, W. M., Dietrick, J., et al. 2004, ApJ, 612, 511, doi: 10.1086/422449

Lendl, M., Bouchy, F., Gill, S., et al. 2020, MNRAS, 492, 1761, doi: 10.1093/mnras/stz3545

Lidov, M. L. 1962, Planet. Space Sci., 9, 719, doi: 10.1016/0032-0633(62)90129-0

Lightkurve Collaboration, Cardoso, J. V. d. M., Hedges, C., et al. 2018, Lightkurve: Kepler and TESS time series analysis in Python, 1.11, Astrophysics Source Code Library. http://ascl.net/1812.013

Lin, D. N. C., & Papaloizou, J. 1986, ApJ, 309, 846, doi: 10.1086/164653

Lindegren, L., Klioner, S. A., Hernández, J., et al. 2020, arXiv e-prints, arXiv:2012.03380. https://arxiv.org/abs/2012.03380

Lithwick, Y., & Naoz, S. 2011, ApJ, 742, 94, doi: 10.1088/0004-637X/742/2/94

Liu, B., Zhang, X., Lin, D. N. C., & Aarseth, S. J. 2015, ApJ, 798, 62, doi: 10.1088/0004-637X/798/1/62

Martinez, M. A. S., Stone, N. C., & Metzger, B. D. 2019, MNRAS, 489, 5119, doi: 10.1093/mnras/stz2464

McLaughlin, D. B. 1924, ApJ, 60, 22, doi: 10.1086/142826

Miller, N., & Fortney, J. J. 2011, ApJL, 736, L29, doi: 10.1088/2041-8205/736/2/L29

Montet, B. T., Crepp, J. R., Johnson, J. A., Howard, A. W., & Marcy, G. W. 2014, ApJ, 781, 28, doi: 10.1088/0004-637X/781/1/28

Moorhead, A. V., & Adams, F. C. 2005, Icarus, 178, 517, doi: 10.1016/j.icarus.2005.05.005

Mordasini, C., Alibert, Y., Georgy, C., et al. 2012, A&A, 547, A112, doi: 10.1051/0004-6361/201118464

Mordasini, C., Klahr, H., Alibert, Y., Miller, N., & Henning, T. 2014, A&A, 566, A141, doi: 10.1051/0004-6361/201321479

Mousis, O., Marboeuf, U., Lunine, J. I., et al. 2009, ApJ, 696, 1348, doi: 10.1088/0004-637X/696/2/1348

Moutou, C., Hébrard, G., Bouchy, F., et al. 2009, A&A, 498, L5, doi: 10.1051/0004-6361/200911954

Müller, S., Ben-Yami, M., & Helled, R. 2020a, ApJ, 903, 147, doi: 10.3847/1538-4357/abba19

Müller, S., Helled, R., & Cumming, A. 2020b, A&A, 638, A121, doi: 10.1051/0004-6361/201937376

Naef, D., Latham, D. W., Mayor, M., et al. 2001, A&A, 375, L27, doi: 10.1051/0004-6361:20010853

Nagasawa, M., & Ida, S. 2011, ApJ, 742, 72, doi: 10.1088/0004-637X/742/2/72

Nagasawa, M., Ida, S., & Bessho, T. 2008, ApJ, 678, 498, doi: 10.1086/529369

Namouni, F. 2010, ApJL, 719, L145, doi: 10.1088/2041-8205/719/2/L145

Naoz, S. 2016, ARA&A, 54, 441, doi: 10.1146/annurev-astro-081915-023315

Naoz, S., Farr, W. M., Lithwick, Y., Rasio, F. A., & Teyssandier, J. 2011, Nature, 473, 187, doi: 10.1038/nature10076

Naoz, S., Farr, W. M., & Rasio, F. A. 2012, ApJL, 754, L36, doi: 10.1088/2041-8205/754/2/L36

Narita, N., Sato, B., Ohshima, O., & Winn, J. N. 2008, PASJ, 60, L1, doi: 10.1093/pasj/60.2.L1

Nesvorný, D., Vokrouhlický, D., & Morbidelli, A. 2007, AJ, 133, 1962, doi: 10.1086/512850

Niemann, H. B., Atreya, S. K., Carignan, G. R., et al. 1998, J. Geophys. Res., 103, 22831, doi: 10.1029/98JE01050

Papaloizou, J. C. B., Nelson, R. P., & Masset, F. 2001, A&A, 366, 263, doi: 10.1051/0004-6361:20000011

Paxton, B., Bildsten, L., Dotter, A., et al. 2011, ApJS, 192, 3, doi: 10.1088/0067-0049/192/1/3

Paxton, B., Cantiello, M., Arras, P., et al. 2013, ApJS, 208, 4, doi: 10.1088/0067-0049/208/1/4

Paxton, B., Marchant, P., Schwab, J., et al. 2015, ApJS, 220, 15, doi: 10.1088/0067-0049/220/1/15

Petigura, E. A. 2015, PhD thesis, University of California, Berkeley

Petigura, E. A., Howard, A. W., Marcy, G. W., et al. 2017, AJ, 154, 107, doi: 10.3847/1538-3881/aa80de

Petrovich, C., Wu, Y., & Ali-Dib, M. 2019, AJ, 157, 5, doi: 10.3847/1538-3881/aaeed9

Pollack, J. B., Hubickyj, O., Bodenheimer, P., et al. 1996, Icarus, 124, 62, doi: 10.1006/icar.1996.0190

Rasio, F. A., & Ford, E. B. 1996, Science, 274, 954, doi: 10.1126/science.274.5289.954

Raymond, S. N., Armitage, P. J., & Gorelick, N. 2010, ApJ, 711, 772, doi: 10.1088/0004-637X/711/2/772

Rein, H., & Liu, S. F. 2012, A&A, 537, A128, doi: 10.1051/0004-6361/201118085

Rein, H., & Tamayo, D. 2015, MNRAS, 452, 376, doi: 10.1093/mnras/stv1257

Ricker, G. R., Winn, J. N., Vanderspek, R., et al. 2015, JATIS, 1, 014003, doi: 10.1117/1.JATIS.1.1.014003

Rossiter, R. A. 1924, ApJ, 60, 15, doi: 10.1086/142825

Salvatier, J., Wiecki, T. V., & Fonnesbeck, C. 2016, PeerJ Computer Science, 2, e55

Santerne, A., Hébrard, G., Deleuil, M., et al. 2014, A&A, 571, A37, doi: 10.1051/0004-6361/201424158

Santerne, A., Moutou, C., Tsantaki, M., et al. 2016, A&A, 587, A64, doi: 10.1051/0004-6361/201527329

Santos, N. C., Israelian, G., & Mayor, M. 2004, A&A, 415, 1153, doi: 10.1051/0004-6361:20034469

Schlafly, E. F., & Finkbeiner, D. P. 2011, ApJ, 737, 103, doi: 10.1088/0004-637X/737/2/103

Schlaufman, K. C. 2010, ApJ, 719, 602, doi: 10.1088/0004-637X/719/1/602

Seager, S., & Sasselov, D. D. 2000, ApJ, 537, 916, doi: 10.1086/309088

Seifahrt, A., Stürmer, J., Bean, J. L., & Schwab, C. 2018, in Society of Photo-Optical Instrumentation Engineers (SPIE) Conference Series, Vol. 10702, Ground-based and Airborne Instrumentation for Astronomy VII, ed. C. J. Evans, L. Simard, & H. Takami, 107026D, doi: 10.1117/12.2312936

Sestovic, M., Demory, B.-O., & Queloz, D. 2018, A&A, 616, A76, doi: 10.1051/0004-6361/201731454

Sheets, H. A., Jacob, L., Cowan, N. B., & Deming, D. 2018, Research Notes of the American Astronomical Society, 2, 153, doi: 10.3847/2515-5172/aadcb1

Shibata, S., Helled, R., & Ikoma, M. 2020, A&A, 633, A33, doi: 10.1051/0004-6361/201936700

Sidis, O., & Sari, R. 2010, ApJ, 720, 904, doi: 10.1088/0004-637X/720/1/904

Smith, J. C., Stumpe, M. C., Van Cleve, J. E., et al. 2012, PASP, 124, 1000, doi: 10.1086/667697

Socrates, A., Katz, B., Dong, S., & Tremaine, S. 2012, ApJ, 750, 106, doi: 10.1088/0004-637X/750/2/106

Spalding, C., Batygin, K., & Adams, F. C. 2016, ApJ, 817, 18, doi: 10.3847/0004-637X/817/1/18

Stumpe, M. C., Smith, J. C., Van Cleve, J. E., et al. 2012, PASP, 124, 985, doi: 10.1086/667698

Sucerquia, M., Ramírez, V., Alvarado-Montes, J. A., & Zuluaga, J. I. 2020, MNRAS, 492, 3499, doi: 10.1093/mnras/stz3548

Tayar, J., Claytor, Z. R., Huber, D., & van Saders, J. 2020, arXiv e-prints, arXiv:2012.07957. https://arxiv.org/abs/2012.07957

Teachey, A., & Kipping, D. M. 2018, Science Advances, 4, eaav1784, doi: 10.1126/sciadv.aav1784

Teske, J. K., Thorngren, D., Fortney, J. J., Hinkel, N., & Brewer, J. M. 2019, AJ, 158, 239, doi: 10.3847/1538-3881/ab4f79

Theano Development Team. 2016, arXiv e-prints, abs/1605.02688. http://arxiv.org/abs/1605.02688

Thompson, S. E., Coughlin, J. L., Hoffman, K., et al. 2018, ApJS, 235, 38, doi: 10.3847/1538-4365/aab4f9

Thorngren, D., & Fortney, J. J. 2019, ApJL, 874, L31, doi: 10.3847/2041-8213/ab1137

Thorngren, D. P., Fortney, J. J., Murray-Clay, R. A., & Lopez, E. D. 2016, ApJ, 831, 64, doi: 10.3847/0004-637X/831/1/64

Torres, G., Konacki, M., Sasselov, D. D., & Jha, S. 2005, ApJ, 619, 558, doi: 10.1086/426496

Trani, A. A., Hamers, A. S., Geller, A., & Spera, M. 2020, MNRAS, 499, 4195, doi: 10.1093/mnras/staa3098

Villanueva, Steven, J., Dragomir, D., & Gaudi, B. S. 2019, AJ, 157, 84, doi: 10.3847/1538-3881/aaf85e

Virtanen, P., Gommers, R., Oliphant, T. E., et al. 2020, Nature Methods, 17, 261, doi: 10.1038/s41592-019-0686-2

Visscher, C. 2012, ApJ, 757, 5, doi: 10.1088/0004-637X/757/1/5

Vogt, S. S., Allen, S. L., Bigelow, B. C., et al. 1994, in Proc. SPIE, Vol. 2198, Instrumentation in Astronomy VIII, ed. D. L. Crawford & E. R. Craine, 362, doi: 10.1117/12.176725

Wahl, S. M., Hubbard, W. B., Militzer, B., et al. 2017, Geophys. Res. Lett., 44, 4649, doi: 10.1002/2017GL073160

Wang, J., Fischer, D. A., Horch, E. P., & Xie, J.-W. 2015a, ApJ, 806, 248, doi: 10.1088/0004-637X/806/2/248

Wang, J., Fischer, D. A., Barclay, T., et al. 2015b, ApJ, 815, 127, doi: 10.1088/0004-637X/815/2/127

Ward, W. R. 1997, Icarus, 126, 261, doi: 10.1006/icar.1996.5647

Winn, J. N. 2010, in Exoplanets, ed. S. Seager (Tucson: Univ. of Arizona Press), 55–77

Winn, J. N., Fabrycky, D., Albrecht, S., & Johnson, J. A. 2010, ApJL, 718, L145, doi: 10.1088/2041-8205/718/2/L145

Winn, J. N., Howard, A. W., Johnson, J. A., et al. 2009, ApJ, 703, 2091, doi: 10.1088/0004-637X/703/2/2091

Wizinowich, P., Acton, D. S., Shelton, C., et al. 2000, PASP, 112, 315, doi: 10.1086/316543

Wong, M. H., Mahaffy, P. R., Atreya, S. K., Niemann, H. B., & Owen, T. C. 2004, Icarus, 171, 153, doi: 10.1016/j.icarus.2004.04.010

Wright, J. T., Marcy, G. W., Butler, R. P., & Vogt, S. S. 2004, ApJS, 152, 261, doi: 10.1086/386283

Wu, Y., & Lithwick, Y. 2011, ApJ, 735, 109, doi: 10.1088/0004-637X/735/2/109

Wu, Y., & Murray, N. 2003, ApJ, 589, 605, doi: 10.1086/374598

Yee, S. W., Petigura, E. A., & von Braun, K. 2017, ApJ, 836, 77, doi: 10.3847/1538-4357/836/1/77